An Investigation of Eclipsing Polars

Michelle Wiehahn

A Thesis

presented to the University of Cape Town

in partial fulfillment

of the NASSP MSc degree

May 20, 2005

Declaration

All work in this thesis which is not reference or disclaimed is my own.

It's the effect of their permanent revolution, their intense circulation, their instantaneous magnetism. – Jean Baudrillard. *Cool Memories*

Acknowledgements

First and foremost, I must thank the National Astrophysics and Space Science Program for giving me the opportunity to participate in their excellent Masters Program. Special thanks must go to Dr. Peter Dunsby, for his incredible devotion to NASSP and its students. Also, to all the lecturers who participate in the program, many of whom interrupt their own lecturing schedules to fly across the country and deliver courses of the highest standard.

Sincere thanks to my supervisors, Dr. Stephen Potter and Prof. Brian Warner:

- Dr. Potter was integral in helping me to obtain, reduce and interpret the observations that form a large part of this thesis. His endless patience is appreciated.

- Prof. Warner has been nothing short of a mentor. His knowledge of the field and willingness to advise, counsel or simply chat has been inspirational.

Kurt Beuermann also deserves thanks as the referee of the paper produced as a result of this work and accepted by Monthly Notices of the Royal Astronomical Society. His comments greatly improved the quality of the paper.

Thanks also to Dr. Patrick Woudt, for always having time to answer silly questions.

Finally, thanks to the National Research Foundation for their financial support.

Abstract

Cataclysmic Variables are introduced, and their structure and evolution discussed. Magnetic Cataclysmic Variables are then investigated, expanding upon the initial discussion to include measurements of the system components and parameters, especially the magnetic field. Techniques specific to eclipsing polars are reviewed.

As an example, a suspected eclipsing polar (SDSS J015543.40+002807.2.) is selected from the Sloan Digital Sky Survey. Photometric and polarimetric observations are obtained. Linear and circular polarization are detected, confirming that it is a new polar. An accurate eclipse ephemeris yields an orbital period of 87.1435 ± 0.0002 min. Assuming a range of mass ratios $0.11 > M_2/M_1 > 0.07$, the inclination lies in the range $85^{\circ} < i < 90^{\circ}$. The circular polarization shows a change in sign, implying that SDSS J015543.40+002807.2 is a two-pole accretor, although the possibility of it being a single-pole accretor cannot yet be ruled out.

The viability of such objects as prospective sources for investigation with the South African Large Telescope is discussed.

Contents

List of Tables

List of Figures

Chapter 1

Introduction

Cataclysmic Variables comprise all the close binaries that contain a white dwarf accreting material, which is transferred from a companion (usually a late main-sequence star). These stars offer a wealth of theoretical challenges: the process of accretion is complex, involving both magnetic fields and discs; the evolution of the system is affected by magnetic braking, gravitational radiation and mass transfer; the point of impact of the accreting material on the white dwarf surface is a source of intense radiation, as is the point where the accretion stream impacts the accretion disc; and many systems undergo novae eruptions as well as disc instabilities. Understanding of these objects is of benefit to a score of scientific disciplines, from stellar evolution to magnetohydrodynamics to particle physics. Chapter 2 introduces these systems in more detail, describing their structure, evolution and observational characteristics.

In this work, the focus is on one particular type of Cataclysmic Variable: the polar. These do not form an accretion disk – rather, the magnetic field of the white dwarf is strong enough that it controls accretion directly onto the surface of the white dwarf. The problem of modelling the lightcurves is simplified in this case by eliminating the need to model the accretion disk. The strong magnetic field dominates much of the physics involved, affecting the flow of material but also the evolution of the system and the spin of the white dwarf. Modelling of such interactions provides a means to better understand stellar evolution and the behaviour of particles in the presence of strong magnetic fields. Chapter 3 reviews the unique structure of these systems and the methods of observation particular to them.

Many techniques have been developed in order to better our ability to understand and predict the nature of polars, but the most powerful probe remains that which nature provides: the eclipse. In a few polars, the inclination of the binary orbital plane to

our line of sight is such that we may observe the eclipsing of one system component by enother. The eclipses allow us to obtain details of the arrangement and relative brightness and sizes of the various components, as well as unambiguously determining such parameters as the binary orbital period. Chapter 4 reviews the techniques used to study eclipsing polars, as well as providing a table of the eleven eclipsing polars known prior to this work.

In Chapter 5, we observe the Sloan Digital Sky Survey Cataclysmic Variable SDSS J015543.40+002807.2, confirming its status as an eclipsing polar. Some of the techniques covered in the previous chapter are applied, and we improve upon previous calculations of the orbital period, as well as investigating a plausible range of system parameters. This chapter appears in the form of the paper which was accepted for publication by Monthly Notices of the Royal Astronomical Society. The paper is entitled "Photometric and polarimetric observations of the eclipsing polar SDSS J015543.40+002807.2; authors are Michelle Wiehahn, Stephen B. Potter, Brian Warner and Patrick A. Woudt. The paper is in press at this time.

Chapter 6 makes concluding remarks. and looks forward to observing these objects with the South African Large Telescope, using the variety of instruments that will be available in the near future.

Chapter 2

Cataclysmic Variables

Cataclysmic variables (CVs) have been reviewed in detail by Hellier (2001) and Warner (1995). Their description of the nature and evolution of CVs forms the basis of this chapter.

A Cataclysmic Variable typically begins life as a main sequence binary system, with an orbital separation of roughly a few hundred solar radii ($R_\odot$), and an orbital period of ~ 10 years. One of the stars, which by convention is labelled the *secondary*, is typically a low-mass (< 1 $M_\odot$) red dwarf. The other, labelled the *primary*, is more massive, and will thus evolve off the main sequence sooner than its companion. In order to understand why this simple inequality so drastically changes the system, we must first understand the concept of Roche geometry.

2.1 Roche Geometry

In a system of two stars, each point in space experiences the gravitational forces of the two stars, as well as the centrifugal 'force' of orbital motion. One may describe the net effect of these forces by means of a three-dimensional system of equipotentials. Projected onto the equatorial plane, these form a two-dimensional system of contours. Near the stellar centres these contours are circular, but on scales comparable to the orbital separation tidal force considerations alter the shape to almost 'teardrop'. There will be a point in space on the major axis between the two stars where the tips of the two facing 'teardrops' meet – the *Inner Lagrangian* or L_1 point. This is a saddle point where the three forces mentioned above are exactly balanced. The equipotentials drawn from this point around the two stars are know as their respective *Roche lobes*. Since it is a saddle point, material at L_1 does not need much of a push to flow from one star's potential well into the other's.

2.2 Common Envelope Phase

As the primary evolves and expands to become a red giant, it fills its Roche lobe, and material at the L_1 point overflows into the secondary's potential well. The secondary is further from the barycentre than the primary, thus the angular momentum of the transferred matter increases. Due to conservation, the orbit loses angular momentum, decreasing the orbital separation. This results in the primary filling its Roche lobe even more, and the effect is a runaway feedback. The primary attempts to dump its entire envelope onto the secondary in the space of only a few years. The secondary cannot assimilate the infalling material at this rate (because it exceeds the Eddington luminosity) and it too fills its Roche lobe, forming a cloud of gas that encompasses both stars. This is known as the *common envelope* phase, and during this time the binary is effectively orbiting within a red giant. The resulting drag on the stars reduces the orbital energy, causing the orbital separation to decrease from ~ 100 $R_\odot$ to ~ 1 $R_\odot$ in about 1000 years. The energy and angular momentum extracted from the binary orbit propels the envelope outward into space, exposing the newly-formed white dwarf (the core of the red giant) and its main sequence companion, surrounded by an expanding planetary nebula. Eventually, this illuminated cloud of gas and dust will dissipate.

2.3 Sustained Mass Transfer

If the orbital separation has decreased sufficiently during this phase of evolution, the secondary will now fill its Roche lobe (if not, magnetic braking will decrease the orbital separation over time, as described below). The material at the L_1 point is given a push in the right direction by the thermal motion of the particles, and it falls into the deeper potential well of the primary. This situation is the opposite of the previous one: the material has lost angular momentum when it arrives at the primary, and the orbital separation increases to compensate, breaking the secondary's contact with its Roche lobe. Hence there must exist some mechanism of orbital angular momentum loss to sustain mass transfer.

This mechanism is provided by magnetic braking from the secondary's stellar wind and magnetic field. The charged particles of the stellar wind are strung along the magnetic field lines before being released into space, and the long lever arm imparts significant angular momentum to the particles. This angular momentum is obtained from the secondary, which being tidally locked extracts it from the orbit. The separation decreases,

allowing the secondary once more to fill its Roche lobe. It is estimated that magnetic braking causes a mass transfer rate, $\dot{M}$, of $\sim 10^{-9}\mathrm{M}_{\odot}\ \mathrm{y}^{-1}$, although individual systems may differ by factors of 10 to 100.

A second source of angular momentum loss is gravitational radiation. A binary system is a gravitational dipole, and thus produces gravitational waves as it orbits. The energy and angular momentum to drive these waves is extracted from the orbit, and decreases the orbital separation. The amount of gravitational radiation produced may be calculated from General Relativity, and is very sensative to period. Gravitational radiation drives mass transfer at $\sim 10^{-10}\ \mathrm{M}_{\odot}\mathrm{y}^{-1}$ for $P_{orb} \sim 2$ h. This is generally outweighed by the magnetic braking effect, but becomes significant in the shortest-period systems.

2.4 Accretion onto the Primary

We now have an image of our CV: a close binary system consisting of an evolved white dwarf (the primary) and a main sequence, late spectral type star (the secondary). The less dense, less massive secondary is distorted by the tidal effect of its companion. As it fills its Roche lobe, material flows ballistically from the L_1 point towards the primary. This, however, is where the family of CVs diverges.

In most CVs, where the magnetic field of the primary is relatively weak, e.g. $B < 5$ MG, the material flowing from the secondary will form a disc around the primary, eventually accreting onto the white dwarf's surface at the disc's innermost edge. However, if the primary's magnetic field is sufficiently high, it may control the accretion to a certain extent. In intermediate cases, a disc can still form, but the final accretion onto the primary takes place via disc material threading onto field lines and flowing along them towards the surface of the star.

In cases where the primary's magnetic field strength is significantly high – derived field strengths lie in the range $11 \leq B \leq 75$ MG – a disc will not form at all. The ballistic stream will thread directly onto the field lines before it ever completes an orbit of the primary. From its threading point it will flow along these field lines to accrete directly onto the primary's surface. The primary's field is also strong enough that it forces the primary to rotate synchronously, with its spin period equal to the binary orbital period. These are some of the principal defining features of a class of CVs know as AM Herculis (AM Her) stars, for the first known example of the class. They are also referred to as *polars*, possibly due to the high degree to which their light is polarised by the magnetic field (although the name was suggested by *Polish* astronomers). In chapters 2 and 3 we

will delve more deeply into their nature and characteristics, and investigate the additional analytical methods available to us in the case of eclipsing systems.

2.5 Outbursts

The luminosities of cataclysmic variables sometimes increase by several magnitudes, the reason for their unusual moniker. The cyclical brightening of a CV by 3 to 5 magnitudes is referred to as a *dwarf nova* outburst, distinguishing it from the more dramatic *nova eruption* which corresponds to a brightening of 8 to 15 magnitudes. The two types of outburst are due to different mechanisms, and originate in different parts of the CV.

The less dramatic of the two, the dwarf nova outburst, is in fact a brightening of the accretion disc. Osaki's model of disc instability (Osaki 1974) shows that it is caused by the mass-transfer rate from the secondary exceeding the disc's ability to transport matter through and onto the primary. The disc becomes destabilised, the viscosity increases, increasing angular momentum transport, and widening the disc. This increases the accretion rate onto the primary, enhancing the luminosity of the system (hence the brightening) and draining the disc of the extra material. The disc drops back into a quiescent state, until the continuing mass transfer causes another instability.

Dwarf nova outbursts are quasi-periodic, and disc-fed CVs experience them many times during their lifetime. Less frequent are the dramatic nova eruptions. These are the events most likely to be noticed as *novae stella* or 'new stars' by the naked eye. CVs that are observed to undergo such an event are labelled *classical novae*. The outburst typically takes 1-3 days to rise to full brightness, but the time taken to decline varies from star to star. The speed of decline is related to amplitude, with the brightest novae declining the fastest.

The cause of *this* eruption originates near the surface of the primary. While a white dwarf is a degenerate star, depleted of hydrogen and made up mostly of helium and/or heavier elements, it is being supplied with material from the secondary. Since the secondary is a main sequence star, the material accreting onto the white dwarf's surface is mostly hydrogen. The surface gravity of the white dwarf is immensely strong, and the material at the base of the accretion layer is compressed and heated under the weight of the gas above. The density at the base of the layer is sufficient to cause degeneracy in the material, forcing the electrons into the lower energy levels. Pauli's Exclusion Principle dictates that no more than two electrons may occupy a single energy level, thus providing an opposing *electron degeneracy pressure*. The temperature increases until

hydrogen burning begins. In normal matter, this release of energy provides an outward thermal pressure, resulting in alleviation of the pressure from above and cooling of the gas. However, in degenerate matter the pressure is determined by density alone, and the energy released by hydrogen fusing to helium only goes to increase the temperature, driving more fusion. The thermal runaway increases its speed, and the temperature will climb to well over 10^8 K. When the Fermi temperature is reached, the degeneracy is suddenly lifted as the electrons switch to a Maxwellian distribution. The material expands catastrophically, brightening the system by many magnitudes. The radioactive nuclei deposit their energy into the shell of gas which is now rapidly expanding outwards from the primary at a rate of ~ 1000 km s^{-1}. The hot shell engulfs the binary, and as it cools and expands the eruption slowly fades.

Nova outbursts are understandably not as frequent as dwarf nova outbursts. However, a CV will undergo many of these cataclysms in its lifetime, usually on repetition time scales much longer than our observational records.

2.6 Orbital Period Distribution

The orbital period of a CV is not only useful for determining the scale of the binary (by Kepler's third law), but may also reveal something of the evolutionary path of CVs. As described in Section 2.3, a CV's orbital separation must in general (but see section 1.6.3) decrease to sustain mass transfer from the secondary. CVs thus appear at some initial orbital period and evolve to shorter periods. Fig. 2.1 shows the distibution of orbital periods taken from Downes et al. (2001). Polars are separated from other CVs and shown in black. An examination of this figure reveals several characteristics of CVs and their evolution.

2.6.1 The Period Maximum

The number of systems decreases noticeably for longer periods. Although not shown in Fig. 2.1, the number of objects with $P_{orb} > 9$ h is only about 7%. This results from the mass restrictions inherent in CVs, i.e. that the primary cannot exceed the Chandrasekhar limit of 1.44 $M_\odot$ and that the secondary must be less massive than the primary. Larger P_{orb} implies larger orbital separation, which increases the size of the secondary's Roche lobe, requiring a more massive secondary to fill it. Thus a restriction on the mass of the secondary is a restriction on P_{orb}.

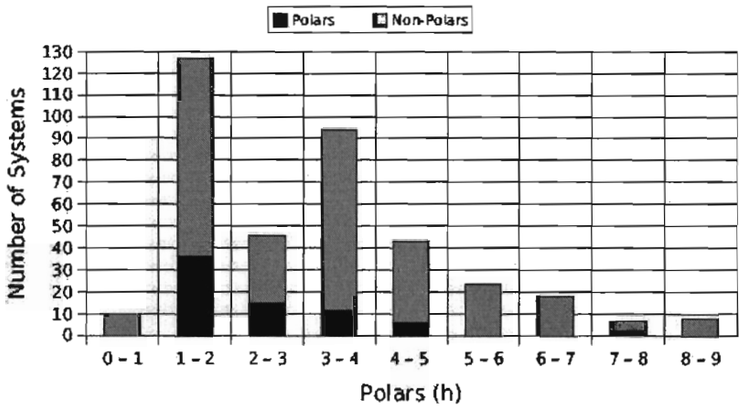

Figure 2.1: Distribution of orbital periods of non-polar CVs (grey) and polars (black).

Long-period systems must contain a secondary which is already evolving towards its red giant stage. Such a star would have a greater volume for the same mass, and would be able to fill a larger Roche lobe than a main sequence star. The secondary is expanding, and the system will thus evolve to longer periods.

2.6.2 The Period Gap

There is a significant relative deficiency of non-magnetic CVs with periods between 2-3 hours. This is referred to as the *orbital period gap*. The cause of this gap is thought to be the disruption of magnetic braking as the secondary becomes fully convective (Webbink & Wickramasinghe, 2002; Wickramasinghe & Ferrario, 2002). The secondary, which is driven out of equilibrium by the mass transfer process, contracts to its equilibrium radius (which it is unable to do during continuous mass transfer) and the binary detaches. This causes the dearth of CVs in the gap. However, gravitional radiation still causes angular momentum loss, and the binary will eventually reattach and reappear below the period gap with a lower mass transfer rate.

Magnetic CVs do not appear to suffer from this magnetic-braking cutoff.

2.6.3 The Period Minimum

There are very few CVs with periods less than 80 min. Upon inspection of actual values of P_{orb}, one finds a minimum period of $\sim$ 75 min for normal hydrogen-rich compositions.

CVs with periods below this minimum (AM CVn stars) have low mass, degenerate secondaries and are helium-rich.

The responsibility for this minimum lies with the secondary: with mass continuously being transferred away from the secondary, its mass will decrease until it becomes degenerate. In such stars, a loss of mass will cause the radius to *increase* rather than decrease. This results in the CV evolving to longer periods, as with those above the period maximum.

As the mass of the secondary continues to decrease, the rate at which gravitational radiation can drive mass transfer also decreases. The binary becomes fainter, and eventually the system detaches.

For further discussion of the period minimum, see Kolb & Baraffe (1999) and Barker & Kolb (2003).

Chapter 3

Polars

The comprehensive reviews on polars presented by Cropper (1990) and Warner (1995) form the basis for this discussion regarding these highly magnetic CVs. We will briefly consider each element of the system, from the component stars to the all-important magnetic field.

The known polars, with magnitude range and period, are presented in Table 3.1.

3.1 The Secondary

3.1.1 Mass and Radius

The secondary in polars, as in other CVs, is a spectral type M or K star, with mass $M_2 \sim 0.1 M_\odot$. Its mass and radius may be calculated directly from the orbital period, given the volume restriction imposed by filling its Roche lobe. Equations for determining M_2 and R_2 from P_{orb} are given in Warner (1995; equations 2.100 and 2.101) and more recently in Smith & Dhillon (1998; equations 9 and 12). The later relations give a slightly better fit for very low mass secondaries.

Polars offer a unique opportunity to observe the secondaries in CVs, in that the spectra are not polluted by lines from an accretion disk. However, intended spectroscopic observations of the secondary are largely dominated by emissions from the primary and the accretion region, making it difficult to obtain these measurements during high accretion states (see section 3.4). During low accretion states, though, the secondary is observable, and phase resolved, high resolution, red and infra-red spectroscopy has been successfully obtained for many secondaries (eg. Ciardi et al. 1998, and references therein). These may be used to determine the radial velocity of the secondary, which is useful in calculating the mass of both stellar components.

3.1.2 Determining Distances to CVs

With secondaries in CVs being very similar in the mean to main sequence stars, it is possible to interpret their photometric lightcurves as one would for a single red dwarf. One may then make use of the Barnes & Evans (1976) formulation for relating the surface brightness in the V band to the unreddened V-R colour in order to calculate the angular diameter of the star. Given this and R_2, it is then possible to calculate the distance to the star. In the absence of uncontaminated V and R band observations, the surface brightness may be calibrated using the molecular TiO band strengths, giving distances that agree well within error margins (Beuermann & Weichhold 1999).

3.1.3 Irradiation of the Secondary

When observing the secondary, it must be taken into account that it is illuminated on one side by radiation from the rest of the system. It is thus important to know the phase of observation, as spectral types estimated from the irradiated hemisphere are likely to be earlier than those from the unirradiated hemisphere. The radiation is also reprocessed by the atmosphere of the secondary, and may be observed as narrow Balmer line emission (~ 200 km s^{-1}) from the chromosphere.

This heating of the secondary, especially around the L_1 point, is thought to be responsible for the change in mass transfer rate, observed as low and high luminosity states. As the surface of the secondary is heated, the mass transfer rate increases, but is eventually checked by the shielding effect of the thickened accretion stream. The reservoir of material around the L_1 point is depleted by this high state, causing a drop in mass transfer rate (corresponding to a low state) until the Roche lobe shrinks sufficiently (King & Lasota 1984).

3.1.4 The Magnetic Field of the Secondary

Current understanding of the evolution of CVs requires a magnetic field of 10^2 - 10^3 G on the secondary, and such a field would play an important part in the synchronisation of the primary. Radio observations of polars AM Her (Chanmugam 1987) and V834 Cen (Wright et al. 1988) suggest the existence of a magnetic field on the secondary if the radio flares are caused by interactions of this field with that of the primary. Further observations of magnetic CVs at radio wavelengths (Pavelin, Spencer & Davis 1994) also point towards the secondary as the source of emissions.

If the secondaries in magnetic CVs are themselves magnetically active, then they

would be expected to emit X-rays. However, with the exception of CVs experiencing episodes of very low $\dot{M}$, any X-ray emission from the secondary would be overwhelmed by that of the primary. It appears unlikely that the secondaries contribute a detectable amount to CV X-ray fluxes (Rucinski 1984; Eracleous, Halpern & Patterson 1991).

3.2 The Primary

3.2.1 Determining the Mass

The primary in polars is a degenerate white dwarf, of mean mass $M_1 = 0.80 \pm 0.14$ $M_\odot$ (Ramsay 2000). Calculating the mass of the primary is more complicated than for the secondary, as it does not fill its Roche lobe and is thus not volume-restricted. As mentioned in the previous section, it is possible to obtain M_1 from Kepler's third law, given the radial velocities of both stars and the inclination of the system. However, this inclination is difficult to determine in non-eclipsing systems.

Although the above method is the most direct in determining the primary mass, others do exist. For example, the degeneracy of the white dwarf results in the radius varying inversely with mass. Thus more massive white dwarfs are smaller, and accreting material will liberate more gravitational energy as it falls into the deeper potential, generating higher temperatures in the accretion region. The temperature of the accretion region may thus provide a lower limit on the white dwarf mass (see Ramsay 2000, and references therein, for a full description of the application of this method).

3.2.2 Synchronisation

The characteristic that separates the primary in polars from that in other CVs is its synchronisation. In most CVs, the effect of material accreting onto the primary, bringing with it angular momentum, is to increase the primary's spin period. In polars, the primary's spin period matches its binary orbital period, to the limits of accuracy provided by the methods employed to measure these periods. This implies one or more torque mechanisms counteracting the accretion torque. Interactions of the primary's strong magnetic field with that of the secondary (in the presence of any plasma of reasonable density) will produce a magneto-hydrodynamic torque. If this torque is sufficient to synchronise the primary, then the interactions of the two fields will maintain that synchronisation.

There are also cases of polars which appear *almost* synchronised – the departure is only $\sim 1\%$. These are the result when the MHD torque is not quite strong enough to synchronise rotation. This may occur if the white dwarf field is weaker than average,

or if the binary separation is larger. It may also be a short-term departure caused by a nova eruption (see section 2.5), in which case the polar should regain synchronisation on a timescale of ~ 1000 years. These systems are known as *asynchronous* polars.

3.3 The Magnetic Field

3.3.1 Field Strength

The strength of the magnetic field is important in determining the system accretion geometry, and its measurement has become one of the primary goals in observing polars. A number of techniques exist for measuring the field strength, based on observable effects of the field.

Zeeman Splitting

When an atom is in the presence of a magnetic field, degenerate energy levels split into separate levels. Thus all spectral lines associated with these levels will also be split into several components, and the degree of this *Zeeman Splitting* is determined by the strength of the magnetic field.

These Zeeman split spectral lines are most easily observed during low states, when the absorption spectrum of the photosphere of the primary is evident. However, the necessity of a low state coupled with a telescope of at least moderate aperture (in order to obtain spectra with sufficient signal-to-noise ratios) has meant that few systems have been measured in this way. Also, the measured spectrum is a flux-weighted mean over the observable photosphere; assumptions must be made regarding the flux distribution in order to apply this method. AR UMa is an example of a system which has been modelled using this method (Schmidt et al. 1996; Ferrario, Wickramasinghe & Schmidt 2003).

It is also possible to observe Zeeman splitting in the cool halo of the accretion flow (e.g. Schmidt, Ferrario, Wickramasinghe & Smith 2001). However, as with the photospheric observations, the interpretation of the data requires some assumptions of the field configuration.

Cyclotron Harmonics

By the laws of electrodynamics, charged particles travelling along a magnetic field line must move along the line in a spiral. This involves circular motion, which produces acceleration, and accelerated charges emit radiation. Thus the spiralling motion produces

what is known as *cyclotron radiation*. For slow-moving particles, this radiation occurs at a characteristic *cyclotron frequency* determined in part by the field strength. For faster-moving particles, the radiation occurs at harmonics of the cyclotron frequency. This radiation produces so-called 'cyclotron humps' in the spectra of polars. By determining which harmonic creates each hump, one may determine the field strength in the region of emission. The spacing of the humps in the spectrum determines the field strength. Also, their breadth, which is partly due to the spread in electron energies, gives some indication of the temperature of the emitting region (e.g. Szkody et al. 2003; Schmidt, Ferrario, Wickramasinghe & Smith 2001).

This method has the advantage of determining the field strength in the accretion region, free of the assumptions required by the Zeeman splitting method. Good signal-to-noise and a wide wavelength coverage is generally sufficient to detect cyclotron harmonics in polar spectra.

Polarisation

Cyclotron radiation is polarised, i.e. the direction of the electric field vector is not random, because of the restriction to spiralling motion around the magnetic field line. One may observe linear polarisation (when the viewing angle is transverse to the field line), circular polarisation (when viewed along the field line) or a mixture of both. The ratio of linear to circular polarisation is dependant only on the viewing angle, the wavelength of observation and the cyclotron frequency (Meggitt & Wickramasinghe 1982; Barrett & Chanmugam 1984). Thus if the ratio is observed at a particular frequency, the viewing angle determined from the geometry, and the harmonic number known, then the cyclotron frequency and thus the field strength may be determined.

Unfortunately this technique has been somewhat restrained by the difficulty in obtaining narrow-band polarimetry. Good signal-to-noise is easier to obtain in broad-band observations, owing to the faintness of the stars. However, initial results have been encouraging (e.g. Cropper, Menzies & Tapia 1986; Piirola, Reiz & Coyne 1987), and narrow-band or spectropolarimetric observations of sufficient accuracy are becoming available with the new generation of telescopes.

This is further discussed in Section 3.6.

3.3.2 Field Configuration

The configuration of the field is usually modelled as an offset dipole. The possibilities of multipolar fields or multiple field configurations in a single magnetic white dwarf are not discounted, but evidence for such fields is difficult to deconvolve from the data. This is largely due to the complicating factor of the magnetic field interactions with accreting material. It is recognised that a dipole field is likely to be a simplification, but it has proven sufficient for the majority of systems.

3.4 The Accretion Stream

Material at the L_1 point is thermally driven to leave the vicinity of the secondary and fall ballistically towards the primary. At some point in its journey towards the white dwarf, the effects of the magnetic field will begin to dominate its motion, eventually controlling it entirely. Due to the fast drop-off of field strength with distance from the primary, we may divide a polar into two regions: where the field has no effect, and where it dominates. The boundary of these two regions is the *magnetosphere*, defined as that volume within which the field strongly affects the flow of mass, energy and angular momentum (e.g., Lamb 1989). The radius of the magnetosphere is determined as the distance from the primary where the magnetic pressure balances the ram pressure of the infalling gas (Davidson & Ostriker 1973). In systems of very high field strength (e.g. AR UMa with $B = 230$ MG) the magnetosphere may reach right up to the L_1 point, controlling the accretion stream for almost its entire journey. This may also occur for systems of $P_{orb} < 2$ h, where the orbital separation is small. In general, for systems with $P_{orb} > 2$ h, the magnetospheric radius will be at some point between the two stars (Mukai 1988). This division of inner and outer zones is aided by the effect of *screening*. At the magnetospheric boundary the field induces electric currents in the infalling material; these currents in turn produce an opposing magnetic field, thereby screening the field from material further out.

We will now consider the behaviour of the accretion stream in the case where a transition between ballistic and magnetic flow occurs at some $r < L_1$. As the gas leaves the L_1 point, it will decrease in density as it accelerates towards the primary. Before reaching the magnetosphere, the stream will pass through a region where the magnetic pressure exceeds the thermal (but not the ram) pressure of the gas. From this point the magnetic field will determine the shape and density of the stream, but not its trajectory.

As the stream continues to accelerate towards the primary, the increasing magnetic pressure of the converging field lines shatters the stream in to small fragments, or 'blobs'. Because of the screening effect, the field cannot easily penetrate these blobs, and they will continue ballistically for a short distance. As the magnetic pressure climbs, the blobs begin to change direction to follow the field lines; collisions in the stream form shocks, energy is radiated away, and material begins to collect in a 'threading' region. This region will extend over a range of radii, owing to the varying blob density, and will contain both blobs and a fine mist of droplets stripped from the blobs' surfaces. The blobs and droplets will then divert from the threading region, along the field lines and towards the white dwarf. The droplets and smaller blobs will be diverted first, with the larger blobs penetrating to deeper regions of the magnetosphere before being threaded onto the field lines. From this point, motion is along the field lines, and generally out of the orbital plane. Depending on the location and extent of the threading region, material may be diverted towards either one or both of the polar regions. In either case, gas threading onto a field line will only be able to reach the primary surface if it does not pass outside of the primary's Roche lobe, as accretion along such field lines would be energetically impossible.

In cases where the magnetosphere extends out to L_1, there are no closed field lines starting at L_1 which still fall within the Roche lobe of the primary. This inhibits accretion directly from L_1, and in observed polars, the stream penetrates for some distance into the magnetosphere before threading onto the field lines.

3.5 The Accretion Region

The accretion region is the small part of the white dwarf onto which the accreting material falls, and in a polar it emits most of the radiation. As described in the previous section, the location of the accretion region(s) is determined by the location and extent of the threading region. Since threading occurs at different points in the threading region, depending on the density of the material, the accretion region will describe an arc at the footpoints of the threaded field-lines. These footpoints are generally near to, but not necessarily at, the magnetic poles. Denser blobs will fall preferentially at one end of the arc, while more diffuse material falls at the other end. The density of the material will determine the nature of the impact.

As the diffuse mist impacts the white dwarf, its kinetic energy is converted to thermal energy, heating it to X-Ray temperatures. The pool of accreted material will expand due

to the heating, resulting in a hot, dense *accretion column* extending above the surface. Incoming material slams into the top of the column, decelerating from supersonic speeds and producing a shock front. The equilibrium height of the column is determined by the requirement that the post-shock flow must have sufficient time to cool and decelerate to match conditions in the white dwarf photosphere. This is determined by the efficiency of the cooling mechanisms:

1. Bremsstrahlung emission: the kinetic energy liberated during deceleration heats the material to $\sim 2 \times 10^8$ K (20 keV), allowing frequent collisions of electrons and ions, causing radiation at mostly hard X-ray wavelengths. The accretion column is optically thin to hard X-rays, and the bremsstrahlung radiation easily escapes through the gas. However, approximately half of this radiation will be directed downwards into the photosphere. Higher energy radiation will be reflected, but some radiation will be absorbed, heating the region around the column until it emits blackbody radiation at soft X-ray temperatures of $\sim 2 \times 10^5$ K (20 eV).

2. Cyclotron radiation: semi-relativistic electrons spiralling around the magnetic field lines emit radiation at characteristic frequencies (see section 3.3.1). The accretion column is optically thick for low harmonics of the cyclotron frequency, but optically thin at higher ones. There will thus be a peak energy for cyclotron radiation. This type of radiation cools the electrons, but not the ions, so two-temperature plasma calculations are required.

3. Compton cooling: relatively low energy photons are scattered by the shocked electrons. This cools the column, but does not result in radiation.

The relative importance of bremsstrahlung radiation vs. cyclotron radiation depends on conditions in the post-shock region, especially on the magnetic field strength and the specific accretion rate. Lamb & Masters (1979) showed that in some cases bremsstrahlung dominates and in others, cyclotron emission dominates. At the extreme of the latter situation, cyclotron cooling is so effective that even the ions, exchanging energy with the electrons, are driven away from a Maxwellian distribution, collapsing the shock structure.

In polars, most of the accreting material is in the form of blobs, rather than diffuse gas. These dense blobs remain unimpeded until striking the photosphere, where they may penetrate for some depth before their kinetic energy is absorbed by the white dwarf. This emerges as blackbody radiation at soft X-ray temperatures of $\sim 2 \times 10^5$ K (20 eV).

This, combined with the reprocessing of hard X-rays into soft X-rays, results in blackbody radiation at soft X-ray temperatures being the dominant source of radiation in polars.

3.6 Polarimetry

As discussed above, cyclotron radiation from polars is highly polarised. Measuring the degree of linear and circular polarisation can paint a vivid picture of the system, and is considered to be the most reliable means of confirming that a system is a polar.

3.6.1 Measuring Polarisation

The state of polarisation of light is normally defined by four *Stokes parameters*, usually written as I, Q, U and V. Given a simple electromagnetic wave propagating in the z direction, the components of the electric vector E are given by (Serkowski 1962):

$$E_x = E_x 0 \sin(\omega t - \epsilon_x) \tag{3.1}$$

$$E_y = E_y 0 \sin(\omega t - \epsilon_y) \tag{3.2}$$

The Stokes parameters are defined as (Chandrasekhar 1950)

$$I = E_{x0}^2 + E_{y0}^2 \tag{3.3}$$

$$Q = E_{x0}^2 - E_{y0}^2 \tag{3.4}$$

$$U = -2E_{x0}E_{y0}\cos(\epsilon_x - \epsilon_y) \tag{3.5}$$

$$V = 2E_{x0}E_{y0}\sin(\epsilon_x - \epsilon_y) \tag{3.6}$$

Thus any beam of light may be considered as consisting of an unpolarised component with Stokes parameters $(I - (Q^2 + U^2 + V^2)^{1/2}, 0, 0, 0)$ and fully polarised component $((Q^2 + U^2 + V^2)^{1/2}, Q, U, V)$ (Chandrasekhar 1950).

The polarisation state may also be described by four other parameters: intensity I (same as the Stokes I), degree of linear polarisation p, position angle θ in the equatorial co-ordinate system, and the degree of circular polarisation q. Parameters are transformed into this system from Stokes parameters as follows (Serkowski 1974):

$$I = I \tag{3.7}$$

$$p = \frac{(Q^2 + U^2)^{1/2}}{I} \tag{3.8}$$

$$\theta = \frac{1}{2}\tan^{-1}(\frac{U}{Q}) \tag{3.9}$$

$$q = V/I \tag{3.10}$$

Expressing the Stokes parameters in terms of this system, we have:

$$Q = Ip\cos 2\theta \tag{3.11}$$

$$U = Ip\sin 2\theta \tag{3.12}$$

$$V = Iq \tag{3.13}$$

Both systems are used in observational astronomy. A device known as a *polarimeter* is used to measure these parameters, by means of a system of optical analysers and retarders (e.g. Cropper 1985). By obtaining these parameters for a particular star, we measure the degree of polarisation of the light, as well as its intensity, producing a wealth of information on the source of the polarisation.

3.6.2 Interpretting Polarisation

The cyclotron radiation responsible for the polarised light is produced in the accretion column. The first attempts to understand the variations in brightness and polarisation observed around the orbital cycle of polars assumed a standard accretion column located at the magnetic pole. This was able to account for gross effects, but not for the asymmetries seen in the observations, or for the wide wavelength range over which polarisation is detected. More complex models (which include the effects of inhomogeneous accretion) have resulted in improvements in the correlation between observation and theory.

Geometrically, the amount of linear or circular polarisation gives a sense of the angle at which we are viewing the accretion column. Simply put, linear polarisation should peak as we view the column most transversely, and circular polarisation should peak when looking most nearly along the field lines leading to the column.

Many systems show a 'double hump' feature: two peaks in the linear and/or circular polarisation. This is characteristic of absorbtion by the accretion stream. When the first peak is higher than the second, it is also an indication that the accretion column leads the magnetic field on the surface of the white dwarf (Ferrario & Wickramasinghe 1990; Potter 1998).

The presence of two accretion regions complicates the issue, often leading to superimposed emissions which are difficult to deconvolve. One measurement which is highly characteristic of a two-pole system is that of a sign-reversal in the circular polarisation.

As one pole disappears over the limb of the primary the other comes into view. We are now looking at the second column's field lines in the opposite sense to those of the first column, with material flowing towards us rather than away. This leads to the sign reversal. However, this may also be caused by an accretion column being viewed from behind just as it passes over the limb of the primary. Observations of sufficient time resolution are often required to ascertain if the polarisation pulses are composed of contributions from one or two poles.

Table 3.1: Polars

Object	Alias	RA (2000)	Dec (2000)	Magnitude Range	Period (min)
EQ Cet	1RXS J012852-233931	01:28:52.47	-23:39:43.2	17.5 V - 18.9 V	92.8
CV Hyi	RX J0132.7-6554	01:32:42.01	-65:54:32.2	19.7 V -	77.8
BL Hyi	H 0139-68	01:41:00.25	-67:53:27.7	14.3 V - 17.4 V	113.6
Hyi	RXS J0154.0-5947	01:54:01.1	-59:47:49.	17.0 V -	-
Cet	SDSSp J015543+002807	01:55:43.38	+00:28:06.7	14.7 p - 17.6 p	87
AI Tri	RX J0203.8+2959	02:03:48.61	+29:59:26.3	15.5 V - 18 V	276.1
Hyi	1RXS J023053-684203	02:30:51.05	-68:42:05.3	16.0 V - 18.0 V	181.8
WW Hor	EXO 023432-5232.3	02:36:11.45	-52:19:13.5	17.6 V - 21.6 V	115.5
VW For	For4; V0252-3037	02:52:51.33	-30:37:43.5	>19.5 j - 20.5 j	-
EF Eri	2A 0311-227	03:14:13.03	-22:35:41.4	13.7 B - 17.7 B	81
VY For	For1; EXO 0329-2606	03:32:04.58	-25:56:55.5	17.5 V - 19.2 V	228.4
UZ For	EXO 033319-2554.2	03:35:28.61	-25:44:22.6	17. V - 20.5 V	126.5
Dor	EUVE J0425-5714	04:25:38.65	-57:14:36.6	19.1 B -	85.8
Eri	1RXS J042556-194534	04:25:55.24	-19:45:30.1	16.6 v -	-
RS Cae	Cae1; RX J0453-4213	04:53:25.46	-42:13:39.6	18.4 V - 19.6 V	-
HY Eri	RX J0501-0359	05:01:46.32	-03:59:20.8	17.5 V - 22.7 V	171.3
V1309 Ori	Ori1; RX J0515+0104	05:15:41.41	+01:04:40.4	15.2 V - 17.3 V	479
UW Pic	Pic1; RX J0531-4624	05:31:35.65	-46:24:05.4	16.4 V - 17.2 V	133.4
BY Cam	H 0538+608	05:42:48.90	+60:51:31.8	14.6 V - 17.5 V	201.3
Lep	RXS J0600.5-2709	06:00:33.24	-27:09:18.4	19 V -	-
Mon	RX J0649.8-0737	06:49:50.84	-07:37:41.1	18.0 B -	263.5
LW Cam	RX J0704.2+6203	07:04:09.90	+62:03:27.9	17.0 V - 20.0 V	97.3
HS Cam	RX J0719.2+6557	07:19:14.45	+65:57:44.8	17 v -	98.2
Mon	RX J0749.1-0549	07:49:10.39	-05:49:25.7	19.0 B -	216
Lyn	SDSS J075240+362823	07:52:40.45	+36:28:23.2	17.7 s -	162
V516 Pup	RX J0803-4748	08:03:45.54	-47:48:45.2	16.2 B - 18.5 B	137.1
VV Pup	1E 0812-1854	08:15:06.73	-19:03:16.8	14.5 V - 18.0 V	100.4
Lyn	1RXS J082051+493433	08:20:50.97	+49:34:31.3	18.0 V - 19.3 V	99.4
EU Cnc	M67-186	08:51:27.21	+11:46:57.0	20.4 V - 21.0 V	125.4
Hya	RXS J0859.1+0537	08:59:09.17	+05:36:54.8	17 V -	-

From the Atlas of Cataclysmic Variables: Living Edition (Downes et al., 2002)

Table 3.1: Polars

Object	Alias	RA (2000)	Dec (2000)	Magnitude Range	Period (min)
Leo	HS 0922+1333	09:24:56.1	+13:20:52.	19 B -	276.5
MN Hya	Hya4; RX J0929-2404	09:29:07.10	-24:05:05.4	17.0 V -	203.4
Leo	RXS J0953.1+1458	09:53:08.16	+14:58:36.4	17.3 V -	103.8
Hya	RX J1002-1925	10:02:11.71	-19:25:37.5	17 B -	106
Hya	RX J1007-2016	10:07:34.61	-20:17:32.7	18.0 V -	210
GG Leo	RX J1015.5+0904	10:15:34.69	+09:04:42.4	16.5 V - 18.8 V	79.9
V381 Vel	RX J1016.9-4103	10:16:58.90	-41:03:44.6	18.5 V -	134.1
WX LMi	HS 1023+3900	10:26:27.52	+38:45:04.2	18 B -	166.9
FH UMa	UMa9; WGA 1047+6335	10:47:09.88	+63:35:13.6	19.4 V -	-
EK UMa	1E 1048.5+5421	10:51:35.23	+54:04:36.0	18.0 v - 20.0 v	114.5
AN UMa	PG 1101+453	11:04:25.71	+45:03:15.0	13.8 B - 20.2 B	114.8
ST LMi	CW 1103+254	11:05:39.75	+25:06:28.9	15.0 V - 17.2 V	113.9
AR UMa	1ES 1113+432	11:15:44.68	+42:58:22.5	13.3 V - 16.5 V	115.9
DP Leo	1E 1114+182	11:17:16.00	+17:57:41.1	17.5 B - 19.5 B	89.8
V1033 Cen	Cen3; RX J1141.3-6410	11:41:22.86	-64:10:14.4	16.6 V -	189.4
EU UMa	RE 1149+28	11:49:55.70	+28:45:07.5	16.5 B - 16.8 B	90.1
GQ Mus	-	11:52:02.52	-67:12:19.7	7.2 v - 18.3 B	85.5
EV UMa	RX J1307+53	13:07:53.85	+53:51:30.0	17.1 V - 20.8 V	79.7
V1043 Cen	RX J1313-3259	13:13:17.12	-32:59:12.2	16 V -	251.4
Vir	SDSS J132411+032050	13:24:11.57	+03:20:50.5	22.1 s -	-
V834 Cen	1E 1405-451	14:09:07.46	-45:17:17.1	14.2 v - 17 v	101.5
Vir	2QZ J142256-022108	14:22:56.36	-02:21:07.2	19.5 b -	-
Vir	2QZ J142438-022739	14:24:39.02	-02:27:38.5	19.5 b -	-
V895 Cen	Cen2; EUVE J1429-38	14:29:27.23	-38:04:10.0	16.5 v - 17.5 V	285.9
MR Ser	PG 1550+191	15:52:47.23	+18:56:27.6	14.9 V - 17. V	113.5
Dra	SDSS J155331+551615	15:53:31.15	+55:16:14.8	18.5 s -	263.5

From the Atlas of Cataclysmic Variables: Living Edition (Downes et al., 2002) – continued from previous page

Table 3.1: Polars

Object	Alias	RA (2000)	Dec (2000)	Magnitude Range	Period (min)
CrB	RX J1554.2+2721	15:54:12.30	+27:21:52.1	16.8 B -	151.9
Ser	1RXS J161008+035222	16:10:07.48	+03:52:33.1	15.9 V -	190.4
Her	SDSS J170053+400358	17:00:53.30	+40:03:57.6	19.4 s -	115.1
V2214 Oph	-	17:12:01.58	-29:37:33.3	8.5 p - 20.5 j	169.2
V1007 Her	RX J1724.0+4114	17:24:06.29	+41:14:09.0	17.6 V -	119.9
Sgr	CXOGC J174532-290552	17:45:32.7	-29:05:52.	-	90.2
V2301 Oph	Oph1; 1H 1752+081	18:00:35.55	+08:10:12.6	16.1 V - 21. V	113
V884 Her	Her5; WGA 1802+1804	18:02:06.53	+18:04:43.3	14.5 V -	113
AM Her	3A 1815+498	18:16:13.33	+49:52:04.2	12.0 V - 15.5 V	185.7
V347 Pav	RE J1844-741	18:44:48.33	-74:18:33.5	15.2 V - 17.6 V	90
Dra	RX J1846.9+5538	18:46:58.93	+55:38:29.3	17.2 R - 20.0 R	128.7
EP Dra	Dra4; 1H 1907+690	19:07:06.13	+69:08:42.4	17.6 V - <21. V	104.6
QS Tel	RE 1938-461	19:38:35.73	-46:12:56.5	15.2 V - 17.4 V	139.9
V1432 Aql	Aql1; RX J1940-1025	19:40:11.47	-10:25:25.1	14.9 V - 18.0 V	201.9
V393 Pav	Pav4; RX J1957.1-573	19:57:11.52	-57:38:22.2	18 V -	98.8
QQ Vul	1E 2003+225	20:05:41.93	+22:39:59.1	14.5 B - 15.5 B	222.5
V349 Pav	Pav1; V2008-6527	20:08:55.79	-65:27:42.6	>18.0 j - 19.5 j	159.7
V4738 Sgr	RX J2022-3954	20:22:37.50	-39:54:12.8	18.5 V - 19.5 V	78
HU Aqr	J2107.9-0518	21:07:58.29	-05:17:39.4	15.3 B - 19.8 V	125
CD Ind	Ind1; EUVE J2115-586	21:15:41.04	-58:40:53.7	16.0 v - 17.8 V	110.9
CE Gru	Gru2; Hawkins V1	21:37:56.38	-43:42:13.1	18.0 B - 20.7 B	108.6
V388 Peg	RX J2157.5+0855	21:57:32.35	+08:55:14.3	17.5 V -	202.5
CP Tuc	Tuc2; AX J2315-592	23:15:19.10	-59:10:28.3	17.1 V -	89
Aqr5	RX J2316-0527	23:16:03.59	-05:27:08.4	17.5 B -	209.4

From the Atlas of Cataclysmic Variables: Living Edition (Downes et al., 2002) – continued from previous page

Chapter 4

Eclipsing Polars - Techniques

4.1 Orbital Period

4.1.1 Obtaining an Orbital Ephemeris

As described in Chapter 2, the orbital period of a binary is an important system parameter. Not only does it provide information about the evolution of CVs, it is also the key to calculating several other system parameters. In eclipsing polars, we can unambiguously extract the binary orbital period, determining it to a high degree of accuracy. It may be seen in Table 4.1 that the orbital period has been calculated for all of the known eclipsing polars.

A greatly simplified model of an eclipse is shown in Fig. 4.1. At time t_1, the source (which may be the white dwarf, the accretion region, or both) begins to pass behind the limb of the secondary. At time t_2 the source is fully eclipsed by the secondary. The interval from t_1 to t_2 is known as the *ingress*. At t_3, the source emerges from behind the secondary, until it is fully out of eclipse at t_4. This interval is the *egress*.

In order to calculate the binary orbital period of a polar, light curves of several eclipses, preferably over a long baseline, must be obtained. The times of mid-ingress or mid-egress of all eclipses are then recorded. A least squares fit of the first degree (i.e. a linear fit) to these times will reveal the period at which the eclipse occurs. This is the binary orbital period, P_{orb}.

Naturally, there are a number of elements which complicate the process. The accuracy of the measurements must be taken into account, and this relies largely on the integration time. The smaller the integration time, the smaller the error in choosing a time for mid-ingress or -egress. These points may also be ambiguous due to a low signal-to-noise ratio. In this case, it is preferable to calculate the time of mid-eclipse and propagate the errors.

This will give a more accurate error estimate for the ephemeris.

After taking all possible errors into account, a linear least squares fit will result in a solution of the form

$$T(HJD) = T_1 + P_{orb} \times E. \tag{4.1}$$

Here, T_1 is some reference time – e.g. the time of the first ingress/egress/mid-eclipse used – and E is the cycle number. An example is Equation 5.1 in Chapter 5:

T(HJD)= $2452969.322093(9) + 0^d.06051635(14)E$

Note that the time is expressed in days, as observations are generally made using heliocentric Julian dates (HJD). The numbers in brackets are the uncertainties.

4.1.2 Confirming Synchronisation

The use of a first degree polynomial fit assumes no change in the period over time. A reliable tool used to check the validity of this assumption is the *observed minus calculated (O-C) diagram.* Here, we subtract the eclipse times calculated (using the ephemeris) from the times measured, and plot these residuals. A polynomial of the correct order should result in an O-C diagram which is a straight line at zero (within error margins). If the line deviates from a straight line, there is some change in the orbital period over time, and a higher-degree polynomial fit may be more appropriate. However, if the change is on a timescale much longer than the baseline of observations, it may not be evident in an O-C diagram. This is partly why a long baseline of measurements is required for unambiguous determination of P_{orb}.

4.1.3 Period-Dependent System Parameters

Some system parameters rely on P_{orb} alone. The mass and radius of the secondary star can be estimated from the empirical mass-period and radius-period relationships of Smith & Dhillon (1998), namely:

$$M_2/M_\odot = (0.126 \pm 0.011)P_{orb}(h) - (0.11 \pm 0.04) \tag{4.2}$$

$$R_2/R_\odot = (0.117 \pm 0.004)P_{orb}(h) - (0.041 \pm 0.018) \tag{4.3}$$

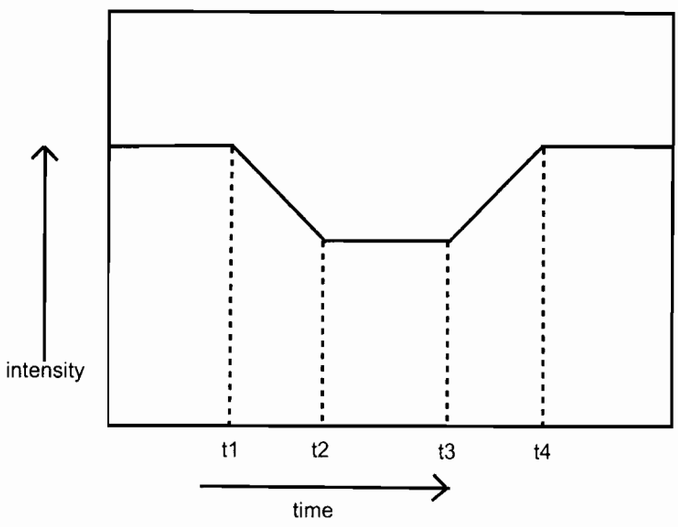

Figure 4.1: Model eclipse

The empirical mass-period and radius-period relations of Warner (1995; equations 2.100 and 2.101 respectively) are also used, although those of Smith & Dhillon have been shown to be more accurate at shorter periods (Smith & Dhillon 1998).

P_{orb} also uniquely defines the mean density of the lobe-filling secondary (Warner 1995):

$$\bar{\rho}(2) = 107 P_{orb}^{-2}(h) \text{ g cm}^{-3} \tag{4.4}$$

Many other system parameters, such as the orbital separation, rely in part on P_{orb}. Also, as indicated in Section 2.6, the orbital period is a measure of the evolutionary stage of the CV. By placing the system in Fig. 2.1, one may compare the system to others in similar stages, and also add to the overall picture of CV evolution. For instance, finding a non-magnetic system with a period that places it in the period gap is significant not only to that system, but to our understanding of period distribution as a whole.

4.2 Binary Inclination

4.2.1 Measuring i

When observing binary systems, the inclination i of the system's orbital plane to our line of sight must be taken into consideration. For example, all measurements of radial velocity yield $v \sin i$, rather than v.

Eclipsing systems provide the most reliable method of determining this inclination, as the system geometry restricts the range of inclinations for which an eclipse is possible. It can be seen in Table 4.1 that i has been calculated to a reasonable degree of accuracy for the majority of known eclipsing polars.

The minimum inclination i_{min} for a grazing eclipse in CVs (treating the secondary as a sphere of volume radius $\mathrm{R}_L(2)$) is

$$i_{min} = \cos^{-1}[R_L(2)/a] \tag{4.5}$$

and may be expressed as a function of q only (Warner 1995). Values of $i_{min}(q)$ may be found in Bailey (1990), and in general we find that $i \geq 74^{\circ}$ for discless CVs (Warner 1995).

An even more accurate measure of i may be obtained by recognising that the duration $\Delta\phi$ of the eclipse is a function only of the mass ratio q and the inclination of the system. This function is not expressible in analytical form for Roche geometry, but Horne (1985) provides a graphical form. This is calculated for discs, but may easily be extrapolated to discless CVs.

Given the inclination of an eclipsing system, and assuming that the secondary fills its Roche lobe, the sizes of the system components may be derived. For the primary/accretion spot, the duration of ingress/egress is a function of the radius of the eclipsed source, as shown in equation 2.92 from Warner (1995):

$$\Delta\phi = \frac{R_1}{\pi a}\left(1 - \frac{\cos^2 i}{\cos^2 i_{min}}\right)^{-1/2} \tag{4.6}$$

Here, we are once again assuming a spherical secondary, and $\Delta\phi$ is the duration of ingress/egress as a fraction of the orbital period.

Similarly, we may use the eclipse duration to estimate the secondary radius. Treating the secondary as a sphere of volume radius $R_L(2)$ (i.e. the volume radius of the secondary's Roche lobe), the relationship between q, i and $R_L(2)$ is given by

$$\sin^2 i \approx \frac{1 - [R_L(2)/a]^2}{\cos^2 2\pi\phi} \tag{4.7}$$

(Warner, 1995; equation 2.64). Here, ϕ is the phase of mid-egress (where phase 0.0 is conventionally the point of mid-eclipse).

4.2.2 High Inclination Systems and Doppler Tomography

Aside from the actual calculation of the binary inclination, the fact that the inclination is high in eclipsing systems is also beneficial to a technique known as Doppler Tomography.

Doppler Tomography was pioneered by Marsh & Horne (1998), as a method to map emission line regions by regarding an observed line profile as the projection of a two-dimensional velocity field along the line of sight. These one-dimensional projections are mapped in two-dimensional doppler space, and this 'tomogram' provides a tool to identify the system components by their characteristic velocity patterns in this space. Doppler Tomography has successfully been extended to discless, magnetic systems (e.g. Schwope et.al. 1999, Schwope 2001), where the lack of a disk and the nature of the accretion stream and accretion region create a dramatically different tomogram.

Firstly, a unique and straight transformation from Doppler space into real space is impossible as both orbital and streaming velocities contribute to the tomograms, making them degenerate in that respect. However, by combining the spatial information from the eclipse with the velocity information from the tomography, it may be possible to produce a genuine picture of the system. This would require extremely good spectroscopic data to match the high time resolution used in eclipse mapping, and is still under development (Hellier 2001).

Secondly, this technique relies on the measurement of velocities from spectra of the CV. As stated in Section 4.2.1, when measuring velocities in an inclined binary system we are actually measuring $v \sin i$, and in systems with low inclination this may result in the velocity curve having very low amplitude. As CVs are relatively faint objects, and the observations are usually high time-resolution, these curves may well be lost to low signal-to-noise ratios. It is thus preferable to observe systems of high inclination, and an eclipsing system ensures this.

Although inversion of the observed line profiles (which are summations of the intensity distribution along the lines of constant radial velocity) can be carried out by standard tomographic processes, the line profiles will be incomplete in the presence of an eclipse. This loss of data is evident in the residuals between observed and calculated trailed spectrograms. However, there are methods which can be applied in order to improve on the goodness of the fit (Schwope et al. 2001), and in general the benefits far outweigh this disadvantage.

4.3 Indirect Imaging of the Accretion Stream

4.3.1 Fitting Stream Models to Eclipse Data

The methods by which the accretion stream in polars couples to the magnetic field (as described in Section 3.4) are complex, and observational constraints are required to

improve the theoretical model. An eclipsing system provides the opportunity to observe the accretion stream indirectly, and a technique for doing so has been developed by Harrop-Allin, Hakala & Cropper (1999), based on work by Hakala (1995).

Assuming one can model or neglect emission from other parts of the system, the light curve is dominated by emission from different parts along the accretion stream. Depending on where in the stream material is heated and emitting radiation, structures will appear in the light curve at certain phases and particularly in the shape of the eclipse. The indirect imaging technique of Harrop-Allin, Hakala & Cropper aims to use these structures to model the stream. Their technique bears close resemblance to Eclipse Mapping of accretion disks in non-magnetic systems (Horne 1985) in that both use photometric eclipse profiles to deduce the distribution of emission between the two component stars, and both make use of the maximum entropy (ME) regularisation to constrain the problem (the latter is necessary as, in general, there are more model parameters than there are data points). The main difference is in the precise ME term used: in Eclipse Mapping the default brightness of an emission point is taken from a uniform image; in this technique the default brightness is the local geometric mean of the adjacent brightnesses on the stream.

The indirect imaging method operates by placing emission points along a pre-set stream trajectory, and then "observing" the model stream through an eclipse of the Roche lobe-filling secondary. The relative brightnesses of the emission points are adjusted to obtain the most locally-smooth stream whose eclipse profile matches the observed eclipse profile. The optimisation is performed using a Genetic Algorithm (GA) to maximise the chance of finding the global optimum (GAs work in a very similar method to biological natural selection: by 'breeding' the 'fittest' solutions from an initial population of random solutions).

The brightnesses of the model points are adjusted to minimise the quantity

$$F = \sum_{i=1}^{N} \left(\frac{model_i - data_i}{\sigma_i}\right)^2 - \lambda \sum_{j=1}^{M} S_j. \tag{4.8}$$

The first summation is the χ^2 for the fitted model light curve. Here, N is the number of data points in the original light curve, $model_i$ is the brightness of the ith model light curve point, $data_i$ is the brightness of the ith point in the original light curve, and σ_i is its uncertainty.

The second summation is the ME regularisation term, where $\lambda > 0$ is a Lagrangian multiplier (which can be changed to adjust the degree of local smoothness required in the

model stream), M is the number of brightness points along the model accretion stream, and S_j is a function of (a) the normalised brightness of the model stream point j and (b) the local geometric mean of the brightness of the emission points neighbouring point j in the model stream.

The χ^2 term ensures that the optimisation finds a solution that is consistent with the original data, and the ME term ensures that the problem is not underconstrained.

Applications of this technique to the bright eclipsing polar HU Aqr in both high-accretion (Harrop-Allin et al. 1999) and low-accretion (Harrop-Allin, Hakala & Cropper 2001) states, as well as V895Cen (Salvi et al. 2002) have provided valuable information about the accretion streams in these systems.

4.3.2 Accretion Stream Mapping Code

A variation on the theme is the *Accretion Stream Mapping* algorithm developed by Vrielmann & Schwope (2001), which uses the complete emission-line light curve to derive spatially-resolved intensity distributions along the surface of a stream modelled as a duodecadon-shaped tube. While the system is rotating, the twelve sides of the stream appear with varying projections and are eclipsed at certain phases either by the stream itself or by the secondary. For the reconstruction of accretion streams using this model, four parameters which describe the geometry of the system (mass ratio q, inclination i, location of the threading point, and orientation of the magnetic axis) have to be determined. Use of the full light curve has proven to constrain these parameters quite well.

4.3.3 Three Dimensional Modelling

What the above methods may lack in complexity is made up for by the 3-D computer model of polars developed by Kube, Gänsicke & Beuermann (2000). The model includes 3-dimensional grid models of the secondary, the primary, the accretion stream and the accretion column, with each component represented by a high number of surface elements, to which brightness values are attributed. The projected surface area of each element for the desired phase may then be calculated, and the flux contributions of all the surface elements may then be summed up to obtain the total flux emitted in the direction of the observer. The light curve can then be fitted to observations in order to derive much more detailed intensity maps of the components of the polar.

4.4 Accretion Stream Eclipses

4.4.1 Light Curve Dips

Eclipsing polars may also exhibit an eclipse by the accretion stream, obscuring either itself or the accretion region. This will appear as a 'dip' in the light curve, during which emission lines are still visible. HU Aqr (Schwope, Schwarz, Sirk & Howell 2001) has very complex soft X-ray light curves: at all occasions they are characterized by a marked on-off behaviour due to the self-eclipse of the accreting pole, and they show eclipses by the companion star, the accretion stream and by an accretion curtain raised between the two stars. The eclipse by the inner accretion stream near to the accretion region results in a broad dip prior to the stellar eclipse. Here, X-rays are being absorbed and scattered by the accretion column just above the accretion spot. The eclipse by the outer accretion stream results in a narrow dip between the broad dip and the stellar eclipse. In a high inclination system like HU Aqr the measured azimuth of the dip centre equals the azimuth of the threading region. The observed width of the dip indicates the azimuthal extent of the threading region. These dips will naturally vary in phase due to changes in the mass accretion rate (and hence of the position of the threading region), and this can be understood in terms of ram pressure and magnetic pressure balancing arguments.

4.4.2 The Stream-Eclipsing Asynchronous Polar V1432 Aql

An eclipse by the accretion stream can thus reveal much about the structure of the stream itself, as well as the accretion spot (e.g. Sirk & Howell 1998). It is thus fortunate that a few polars which do not quite have the inclination necessary for a stellar eclipse may still experience eclipses by the stream (e.g. V884 Her; Greiner, Remillard & Motch 1998). These objects are not classified as eclipsing polars (although the term 'stream-eclipsing polar' is often used), but they will yield more information than systems which experience no eclipse of any kind. An illustrative case is that of V1432 Aql, an asynchronous polar.

Asynchronous polars are interesting puzzles: periods extracted from the light curves are often sidebands and/or harmonics of the underlying P_{orb} and P_{spin} due to pole switching and migration of the accretion footpoints, making their interpretation more difficult. The presence of an eclipse in such a system is useful as successive light curves portray an advancing configuration between the stream and stellar magnetosphere. An extensive observational program could in principle track not only the accretion footpoint(s) across the white dwarf but also the gas trajectory that gives rise to those variations. Schmidt & Stockman (2001) found that the dips in the light curve of V1432 Aql were due to an

eclipse by the accretion stream, allowing them to apply these techniques. This immediately provided not only an orbital period, but also information about the stream, the accretion spot, and the synchronisation rate.

Table 4.1: Eclipsing Polars

Name	Alias	P_{orb} (min)	B (MG)	i (degrees)	M1 ($M_\odot$)	M2 ($M_\odot$)	references
WW Hor	EXO 023432-5232.3	115.5		74 ± 5	0.7:		1,2,3
UZ For	EXO 033319-2554.2	126.5	53,75:	86 ± 5	$0.7_p \pm 0.1$, $> 0.93_s$	0.14_p, 0.16_s	1,4,5,6,7
HY Eri	RX J0501-0359	171.3	~ 25	75 ± 3	$0.43_s \pm 0.1$	0.36	1,8
V1309 Ori	Ori1; RX J0515+0104	479	62		< 0.6		1,9
HS Cam	RX J0719.2+6557	98.2		79 ± 3	$0.75 \pm 0.1_s$	$0.13 \pm 0.05_s$	1,10
MN Hya	Hya4; RX J0929-2404	203.4	42	70-78	0.6-1.44:	0.31	1,11,12
DP Leo	1E 1114+182	89.8	31,59	79.6	0.71_p	0.106_p	1,13,14,15
V895 Cen	Cen2; EUVE J1429-38	285.9		81	0.82	0.46_s	1,16
V2301Oph	Oph1; 1H 1752+081	113	7_z	80 ± 2	$0.9_s \pm 0.1$	0.185_s	1,17,18
EP Dra	Dra4; 1H 1907+690	104.6	16_z	80:	0.43 ± 0.07	0.133_s	1,19,20
HU Aqr	J2107.9-0518	125	37	85 ± 5	$\sim 0.9_s$	$\sim 0.3_s$	1,21

Notes: s spectroscopic determination; z from Zeeman features; p polarimetric determination; (1) Downes et al. (2001); (2) Bailey et al. (1988); (3) Beuermann et al. (1987); (4) Ferrario et al. (1989); (5) Bailey & Cropper (1991); (6) Beuermann et al. (1988); (7) Schwope et al. (1990); (8) Burwitz et al. (1999); (9) Shafter et al. (1995); (10) Tovmassian et al. (1999); (11) Ramsay & Wheatley (1998); (12) Buckley, Ferrario, Wickramasinghe & Bailey (1998); (13) Biermann et al. (1985); (14) Cropper & Wickramasinghe (1993); (15) Bailey et al. (1993); (16) Stobie et al. (1996); (17) Barwig et al. (1994); (18) Ferrario et al. (1995); (19) Remillard et al. (1991); (20) Schwope & Mengel (1997); (21) Schwope et al. (1993).

Chapter 5

The Eclipsing Polar SDSS0155

5.1 abstract

We present photometric and polarimetric follow-up observations of the eclipsing Sloan Digital Sky Survey cataclysmic variable SDSS J015543.40+002807.2. Linear and circular polarization were detected, confirming that it is a new polar (AM Herculis system). An accurate eclipse ephemeris yields an orbital period of 87.1435 ± 0.0002 min. Assuming a range of mass ratios $0.11 > M_2/M_1 > 0.07$, the inclination lies in the range $85^{\circ} < i < 90^{\circ}$. The circular polarization shows a change in sign, implying that SDSS J015543.40+002807.2 is a two-pole accretor, although the possibility of it being a single-pole accretor cannot yet be ruled out.

5.2 Introduction

Cataclysmic variables (CVs) are close binary systems where matter is being transferred from the main sequence secondary (usually a late spectral type star) onto the evolved primary (white dwarf). AM Herculis systems (or polars) are those where the primary has a magnetic field strength sufficiently high to synchronise its spin period with the binary orbital period, and to control the accretion of material. The magnetic field prevents the formation of a disc, and the stream impacts directly onto an accretion region on the surface of the primary.

Systems of high inclination ($\geq 74^{\circ}$ for discless CVs; Warner 1995) will result in a total or partial eclipse of the primary and/or the accretion region. These systems are highly sought after, as eclipsing systems allow accurate and unambiguous determination of the orbital period, and phase-dependent phenomena may then be referenced to this period. Period-dependent empirical formulae for parameters such as secondary mass

and radius (e.g. Warner 1995; Smith & Dhillon 1998) may be solved. The features of the eclipse, such as duration and shape, can place restrictions on some of the system parameters, and aid in describing the system geometry. Techniques which make use of these advantages include indirect imaging of the accretion stream using photometric eclipse profiles (Harrop-Allin, Hakala & Cropper 1999) and observation of X-ray eclipses to obtain detailed information about the accretion region, stream and curtain (Schwope et al. 2001). The high inclinations make these systems particularly favorable for radial velocity studies and Doppler imaging (Schwope 2001).

Due to the strong emissions of the accretion regions, polars are traditionally discovered in soft X-ray and EUV surveys using satellites such as ROSAT (e.g. Beuermann & Burwitz 1995). However, systems in low accretion states or systems with little X-ray emission may have been overlooked. The Sloan Digital Sky Survey has been successful in discovering new CVs, despite its main focus being on spectroscopy of extragalactic objects. It remains to be seen if the new polars among them were simply in a low state during the ROSAT surveys or that their cooling mechanisms are not X-ray dominated. Some of these new CVs are to be found in the first data release (Szkody et al. 2002), which describes the survey and lists 19 new CVs from spectra obtained during December 2000. Among these was SDSS J015543.40+002807.2 (hereafter SDSS0155), an eclipsing system with characteristics suggestive of an AM Her star.

SDSS0155 was followed up during the Nordic-Baltic Research Course "Astrophysics of Interacting Stars" with the Nordic Optical Telescope, in August 2002 (Dubkova, Kudryavtseva & Hirv 2003). They were able to collect only a single light curve of ~ 101 min duration using 60 s exposures and 7 s readout time. Their observations yielded several system parameters, and they concluded that further photometric observations would be required to pin down the system geometry, as well as polarimetric observations to confirm that SDSS0155 is a polar.

SDSS0155 was further observed as part of the University of Cape Town's faint CV survey (Woudt, Warner & Pretorius 2004): the data obtained are included here.

5.3 Observations

5.3.1 Polarimetry

SDSS0155 was observed on five nights during November/December 2003 (see Table 5.1) using the South African Astronomical Observatory (SAAO) 1.9-m telescope and the UCT Polarimeter (UCTPol; Cropper 1985). The UCTPol was operated in all Stokes

Table 5.1: Log of observations. UCT CCD is the University of Cape Town CCD camera. UCTPol is the University of Cape Town photo-polarimeter. All observations are unfiltered.

Date	Instrument	Resolution (s)
04 Oct 2003	UCT CCD	45
05 Oct 2003	UCT CCD	45,10
25 Nov - 28 Nov 2003	UCTPol	10,1
01 Dec 2003	UCTPol	10,1

Table 5.2: Table of eclipse timings. Ingress, egress and mid-eclipses are HJD-2452000.

Ingress	Egress	Mid-Eclipse	Cycle
917.39722(73)	917.40086(74)	917.39904(104)	-858.0
918.36554(52)	918.36918(52)	918.36736(74)	-842.0
918.42609(12)	918.42956(12)	918.42782(16)	-841.0
969.32032(12)	969.32390(16)	969.32211(20)	0.0
969.38081(01)	969.38440(01)	969.38261(02)	1.0
969.44137(16)	969.44491(07)	969.44314(18)	2.0
969.50185(01)	969.50544(01)	969.50364(02)	3.0
970.28844(35)	970.29218(08)	970.29031(35)	16.0
970.34903(09)	970.35262(13)	970.35082(16)	17.0
970.40948(14)	970.41327(21)	970.41137(25)	18.0
971.31733(01)	971.32092(02)	971.31913(02)	33.0
971.37786(01)	971.38144(02)	971.37965(02)	34.0
972.34610(12)	972.34974(08)	972.34792(14)	50.0
975.31141(01)	975.31501(01)	975.31321(02)	99.0

mode, i.e. simultaneous linear and circular polarimetry, and photometry. White light, defined by an RCA31034A GaAs photomultiplier response 3500 – 9000 Å, observations were undertaken. Polarization standard stars (Hsu & Breger 1982) were observed during the nights to set the position angle offsets. Non-polarized standard stars and calibration polaroids were observed to set the efficiency factors. The data were reduced as described in Cropper (1997).

5.3.2 Photometry

SDSS0155 was observed for two nights in October 2003 (Table 5.1) using the SAAO 1.9-m telescope and the University of Cape Town CCD (UCTCCD; O'Donoghue 1995) used in frame transfer mode and white light. The first night's data were obtained at a time resolution of 45 s throughout. On the second night a resolution of 10 s was used during eclipse. The data have been sky subtracted and extinction corrected. They have also been flux calibrated by observing hot white dwarf standards, providing magnitudes roughly on the V scale, good to ~ 0.1 mag (Woudt, Warner & Pretorius 2004).

SDSS0155 was later observed on five nights during November/December 2003 (Table 5.1), using the SAAO 1.9-m and the UCTPol. The photometry was obtained as part of the polarimetric observations (see section 2.1), at a time resolution of 10 s out of eclipse, and 1 s during eclipse. These are not flux calibrated but are sky subtracted and extinction corrected.

Combining the UCTCCD and UCTPol data, a total of 14 eclipses were observed.

5.4 Analysis

5.4.1 Photometry

The upper plot of Fig. 5.1 shows all of the UCTPol photometry folded on the ephemeris (given in equation 5.1 below). Upon inspection, we find no evidence of the 'far-field accretion stream dip' suggested by Dubkova et al. (2003).

The gross orbital features show a bright and faint phase typical of polars with one accretion spot, which is self-occulted by the primary for part of the orbit.

The fall to minimum of the bright phase is visibly more rapid than the rise to maximum. A single, extended, arc-shaped accretion region with asymmetrical brightness would explain this feature (e.g. Cropper 1990). However, the asymmetry could also be attributed to a two-pole system where the leading brighter pole is slightly ahead in longitude than the trailing pole.

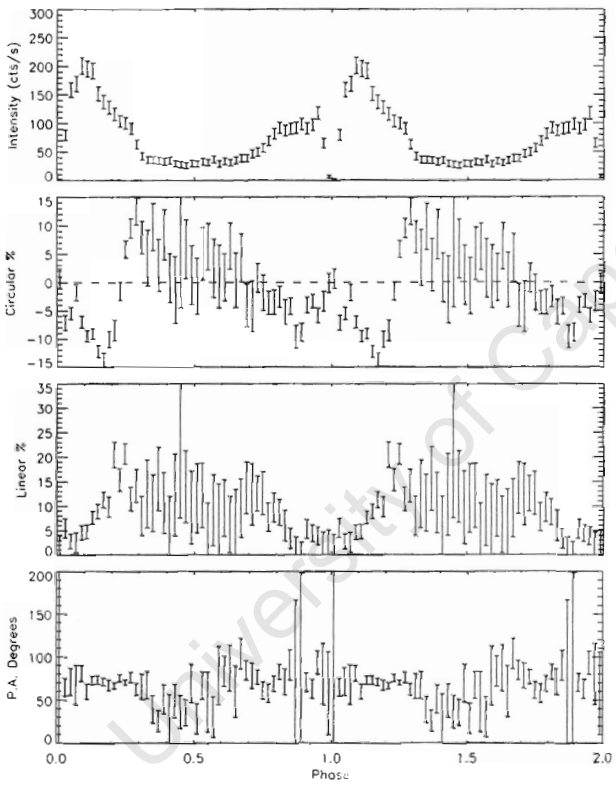

Figure 5.1: Photometric and polarimetric data (white light) binned and folded on the ephemeris in equation 5.1.

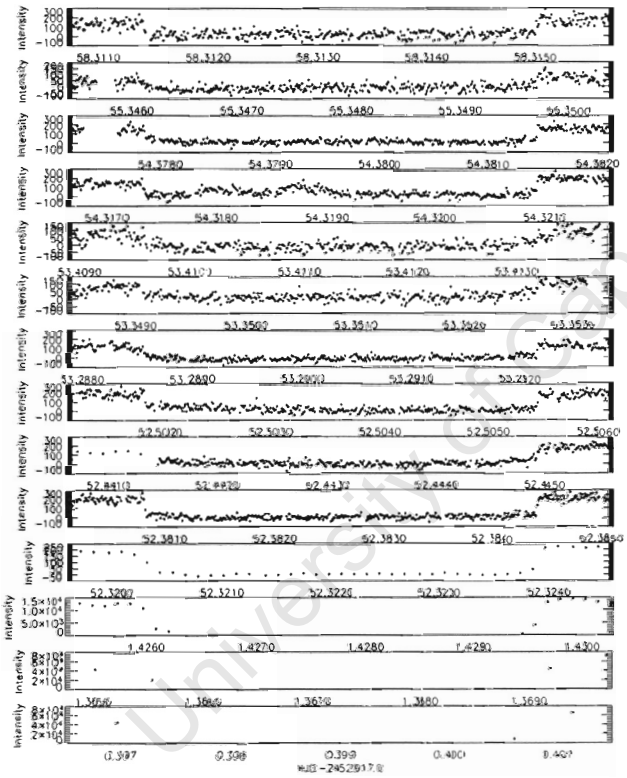

Figure 5.2: Observed eclipse profiles.

5.4.2 Polarimetry

The circular and linear polarization plots (binned and folded on the ephemeris in equation 5.1) are shown in Fig. 5.1. As with the photometry, the polarized light curves are typical of polars and can be understood as a combination of self-occultation and cyclotron beaming of the radiation from an accreting hot spot.

The circular polarization plot shows both negative and positive polarization, with the negative polarization showing a 'double-hump' feature characteristic of absorption by the accretion stream. The peak at phase 1.2 is higher than that at phase 1.9, an indication that the accretion spot is leading the magnetic pole on the surface of the primary (Ferrario & Wickramasinghe 1990; Potter 1998).

The change in sign of the circular polarization is usually interpreted as an indication of a two-pole accretor. However, since the reversal occurs only briefly at the end of the photometric bright phase, a single-pole accretion model is still viable. A sufficiently tall shock can be viewed with the field lines facing away from the observer as the region disappears over the limb of the primary. During this short interval we are effectively viewing the accretion column from underneath thus reversing the sign of circular polarization.

The linear polarization shows two peaks, the first coinciding (in orbital phase) with the sign-reversal in the circular polarization, and the second coinciding with the start of the bright phase. The first peak appears higher than the second, again indicating that the accretion region leads the magnetic pole (Ferrario & Wickramasinghe 1990; Potter 1998). The features of the linear polarization plot may be explained by both the single- and two-pole accretion models.

A test to distinguish between the two possibilities would be to obtain phase resolved spectroscopic observations of SDSS0155. If it is a two-pole accretor there will be two sets of cyclotron harmonics; if it is a single-pole accretor there will be only one set. However, this effect does rely on there being sufficient difference in field strength at the two poles.

The position angle variations (lowest plot in Fig. 5.1) are uninformative due to the low count rate of the linear polarization.

5.4.3 Eclipse Features

In Fig. 5.2, all 14 observed eclipses are shown, with the most recently observed at the top. The bottom three panels are from the UCTCCD data, while the remainder are from the UCTPol data. The eclipses have been aligned using the ephemeris of equation 5.1.

The UCTPol data offer higher resolution during eclipse, and from them we see that

Table 5.3: Summary of parameters calculated for typical primary masses.

Parameter	$M_1 = 0.66 M_\odot$	$M_1 = 0.94 M_\odot$
q	0.11	0.07
i	85^o	90^o
θ	25^o	0^o
a (cm)	$(4.1 \pm 1.1) \times 10^{10}$	$(4.5 \pm 1.2) \times 10^{10}$
R_{source} (cm)	$(6.6 \pm 2.5) \times 10^7$	$(8.2 \pm 3.1) \times 10^7$
R_1 (cm)	8.1×10^8	5.9×10^8

the time taken for the primary to be eclipsed is on the order of a few seconds. Thus only the 1 s time resolution data were used in calculating an average ingress/egress time, with the result:

- average ingress time: 3.2 ± 1.2 s
- average egress time: 2.9 ± 1.1 s

where the errors are standard deviations. A weighted average of the two times yields a phase range $\Delta\phi = 5.8 \times 10^{-4}$ for ingress/egress.

We calculate the average of the total eclipse duration to be 312.3 ± 6.5 s which corresponds to a phase range $\Delta\phi = 0.0597 \pm 0.0012$.

5.4.4 An Eclipse Ephemeris

The resolution of the eclipse ingresses and egresses varies over the data set (see Table 5.2), largely due to differences in time resolution. Thus the times of mid-eclipse were chosen for the ephemeris, as they will provide a more accurate estimate of the errors. A linear least squares fit to the midpoints of the eclipses gives the following eclipse ephemeris:

$$T(HJD) = 2452969.322093(9) + 0^d.06051635(14)E \quad (5.1)$$

i.e. an orbital period of $P_{orb} = 87.1435 \pm 0.0002$ min. Szkody et al. (2002) calculated the orbital period spectroscopically; their estimate of ~ 87 min agrees with our value.

Fig. 5.3 shows the O-C diagrams for the two sets of data. There is no evidence supporting the need for a second order term in the fit.

5.4.5 The System Geometry and Dimensions

We now use the eclipse parameters to investigate the system geometry and dimensions.

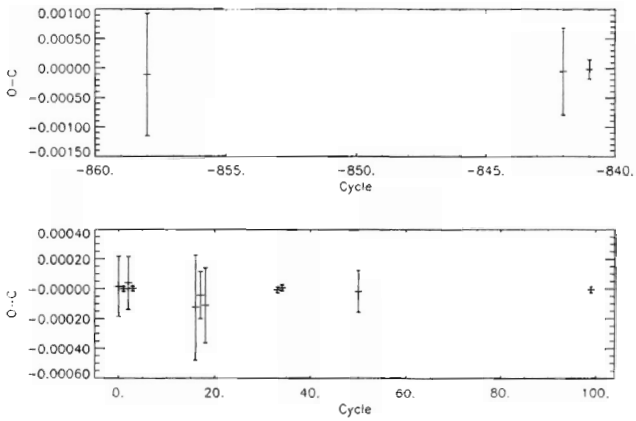

Figure 5.3: Residuals of the times of mid-eclipse, with respect to the best- fitting linear ephemeris.

The mass and radius of the secondary star can be estimated from the empirical mass-period and radius-period relationships of Smith & Dhillon (1998; equations 9 and 12 respectively), i.e.

$$M_2/M_\odot = (0.126 \pm 0.011)P_{orb}(h) - (0.11 \pm 0.04) \tag{5.2}$$

and

$$R_2/R_\odot = (0.117 \pm 0.004)P_{orb}(h) - (0.041 \pm 0.018) \tag{5.3}$$

which give $M_2/M_\odot = 0.07 \pm 0.03$ and $R_2/R_\odot = 0.13 \pm 0.06$ for SDSS0155.

Ramsay (2000) gives a mean value of $M_1/M_\odot = 0.80 \pm 0.14$ for the white dwarf mass in polars. We will thus adopt a range $0.66 < M_1/M_\odot < 0.94$ for our primary mass, in order to make a first estimate of further system parameters. This, combined with the result from equation 5.2, yields a mass ratio $0.11 < q < 0.07$.

Next we use the duration of total eclipse of the primary, which is a function only of the mass ratio ($q = M_2/M_1$) and the inclination (i). This cannot be expressed analytically, but Horne (1985) presents a graph of the relationship as a function of eclipse width. Given this, and the eclipse width $\Delta\phi = 0.0597$, in conjunction with our range of q, the inclination lies in the range $85^\circ < i < 90^\circ$. The uncertainty in q, from the relatively large uncertainty in equation 5.2, translates to an uncertainty of only 0.5° in the lower boundary of i.

Given the range of inclination angle, we estimate a range for the co-latitude of the accretion spot (assuming only one spot; see Section 3.2). We adopt the Visvanathan &

Wickramasinghe (1981) approximation that the accretion region is a point source near to the dipole axis, eclipsed by the primary for a fraction α of the orbital period. If θ is the co-latitude of the dipole axis with respect to the rotation axis – which is assumed to be normal to the orbital plane – then the relation between these factors and the inclination may be expressed as:

$$\cot i = \cos \pi\alpha \tan \theta \tag{5.4}$$

(Visvanathan & Wickramasinghe 1981; equation 1). From Fig. 5.1 the fraction of the orbit during which the primary obscures the accretion region is $\alpha = 0.4$. This yields a range $16^{\circ} < \theta < 0^{\circ}$ for the co-latitude of the accretion spot. However, this model makes the assumption that there is no accretion column, which extends vertically above the accretion region and would thus minimise the observed α. The true value of alpha is thus slightly larger than that measured from the lightcurve. Assuming an accretion column with vertical extent above the surface of ~ 0.01 R_1, the value of α is increased by 0.04. This leads to a range in co-latitude $25^{\circ} < \theta < 0^{\circ}$.

We use the Nauenberg mass-radius relation for helium white dwarfs (Nauenberg 1972; equation 2.82 in Warner 1995), and the range of probable primary masses above, to obtain a range $8.1 \times 10^8 > R_1 > 5.9 \times 10^8$ cm for the primary radius. This may represent a slight underestimate (by a few percent of R_1) if the primary is a carbon white dwarf.

The separation between the centres of mass of the binary components is given by

$$a = 3.53 \times 10^{10} (M_1/M_{\odot})^{1/3} (1+q)^{1/3} P_{orb}^{2/3}(h) \tag{5.5}$$

from Warner (1995; equation 2.1b). A primary mass in the range $0.66 < M_1/M_{\odot} < 0.94$ then gives a separation of $(4.1 \pm 1.1) \times 10^{10} < a < (4.5 \pm 1.2) \times 10^{10}$ cm.

Given a and the phase range $\Delta\phi$ for ingress/egress, we can calculate the radius of the eclipsed source, from equation 2.92 of Warner (1995):

$$\Delta\phi = \frac{R_{source}}{\pi a} \left(1 - \frac{\cos^2 i}{\cos^2 i_{min}}\right)^{-1/2} \tag{5.6}$$

Values for $i_{min}(q)$ – the minimum inclination allowable (i.e. for a grazing eclipse) – may be found in Bailey (1990). Propagating the errors, we obtain $(6.6 \pm 2.5) \times 10^7 < R_{source} < (8.2 \pm 3.1) \times 10^7$ cm. Equation 5.6 assumes that the source is the spherical primary. However, the source is likely to be the arc-shaped accretion region, in which case R_{source} gives some sense of scale (along the eclipse path) for this region, but is not a 'radius'. We obtain $R_{source} \sim 10^{-1} R_1$, as expected for an accretion region on the surface of the white dwarf (Ferrario & Wickramasinge 1990).

In Table 5.3, we summarise the parameters calculated in this section, for the upper and lower bounds of the estimated primary mass range.

5.5 Summary and Conclusions

Our photometric and polarimetric observations confirm that SDSS0155 is a new polar, with an orbital period of 87.1435 ± 0.0002 min, placing it shortward of the orbital period gap. Assuming a range of mass ratios $0.11 > M_2/M_1 > 0.07$, the inclination lies in the range $85^{\circ} < i < 90^{\circ}$. The change in sign of the circular polarization may be interpreted as the system being a two-pole accretor, although the possibility of single-pole accretion cannot yet be ruled out. Spectroscopic observations may resolve this issue.

Chapter 6

Conclusion: Looking Forward to SALT

There is no question of the desirability of eclipsing polars as targets for observation. They provide unambiguous determination of important system parameters, a fiducial against which to compare phase-dependant phenomena, and an invaluable probe into the structure of polars.

It is true that there are specific challenges involved in observing such objects. High resolution – in both time and wavelength – is often a necessity, but produces low signal-to-noise ratios for these faint stars. Yet, with the advent of bigger and better telescopes, and finer equipment, we begin to meet these challenges head-on.

In South Africa, we are in a prime position to discover and examine eclipsing polars. Together with our partners in Germany, Poland, New Zealand, America and the U.K., we are currently building the South African Large Telescope (SALT). The primary reflective surface is a hexagonal mirror array 11 metres across, making SALT the largest single telescope in the southern hemisphere (a full description of the telescope, including a list of published papers, can be found at the official website: http://www.salt.ac.za).

The primary mirror is spherical, with an optical axis tilted to 37 degrees from the vertical. It can rotate through 540 degrees in azimuth. Positioned $\sim$ 13 m above the mirror is a tracker and an optical payload, looking down at the mirror. The tracker moves across the mirror on a virtual spherical focus surface, allowing sky-objects to be "followed" as the earth rotates, without adjusting the azimuth angle for a period of up to two hours. This gives the telescope an annulus-shaped observing area in the sky, 12 degrees wide between declination angles of approximately -75 degrees and +10 degrees. The disadvantage of this observing area is that objects can only be tracked continuously for about 50 minutes to a maximum of about 3 hours, depending on the position of the

object (i.e. where it crossed the window of regard). Yet this makes short-period objects like polars perfect for observation with SALT, as most polars fall below the period gap (putting their orbital periods in a range of about 2 hours to 80 minutes).

SALT will also have the necessary instrumentation and resolution needed to successfully observe eclipsing polars. The SALT design is optimised for high-resolution spectroscopic measurements: both the High Resolution Spectrograph (HRS) and the Prime Focus Imaging Spectrograph (PFIS) will be able to deliver observations of the quality required by many of the techniques mentioned in previous chapters. In addition, large aperture polarimetric optics will also provide for spectropolarimetric capability in all the spectroscopic modes (Buckley 2001).

Future plans for the instumentation include the possibility of a fibre-fed superconducting tunnel junction (STJ). The STJs are a new generation of detectors that record not only the arrival time of incident photons, but also their energy (Perryman et al, 1993). An STJ device on the William Herschel Telescope, known as S-Cam2 (Rando et al. 2000), has been successfully used to observe eclipsing polars HU Aqr (Bridge et al. 2002) and UZ For (Perryman et al. 2001). The high time resolution, high efficiency, large dynamic range and modest energy resolution afforded by this system allow a direct probing of the energy dependance of the intensity variations across the eclipse. This includes investigation of the details of the ingress and egress light curves, whose structure provides important diagnostics of the emission mechanism (Perryman et al. 2001). There is no doubt that the inclusion of such a device on SALT will benefit the observation of polars in general, and of eclipsing polars in particular.

Bibliography

[1] Bailey J., 1990, The Masses of Cataclysmic Variables - A Statistical Approach, *Mon. Not. R. Astron. Soc*, **243**, 57

[2] Bailey J. & Cropper M., 1991, The eclipse light curves of UZ For, *Mon. Not. R. Astron. Soc.*, **253**, 27

[3] Bailey J, Wickramasinghe D.T., Hough J.H. & Cropper M., 1988, EXO 023432-5232.3 - an eclipsing AM Herculis binary, *Mon. Not. R. Astron. Soc*, **234**, 19

[4] Bailey J., Wickramasinghe D.T., Ferrario L., Hough H.J. & Cropper M., 1993, Changes of Accretion SPOT Longitude in Eclipsing Am-Herculis Binaries, *Mon. Not. R. Astron. Soc*, **261**, L31

[5] Barker J. & Kolb U., 2003, The Minimum Period Problem in Cataclysmic Variables, *Mon. Not. R. astron. Soc*, **340**, 623

[6] Barnes T.G. & Evans D.S., 1976, Stellar Angular Diameters and Visual Surface Brightness.I. Late Spectral Types, *Mon. Not. R. Astron. Soc*, **174**, 489

[7] Barrett P.E. & Chanmugam G., 1984, Polarized radiation from hot plasmas and applications to AM Herculis binaries. II - Effect of collisions and Thomson scattering, *Astrophys. J.*, **278**, 298

[8] Barwig H., Ritter H. & Barnbanter O., 1994, 1H 1752+081: A new eclipsing probable AM Herculis type binary, *Astronomy & Astrophysics*, **288**, 204

[9] Beuermann K. & Burwitz V., 1995, AM Herculis Binaries in the ROSAT ERA, *ASP Conference Series*, **85**, 99

[10] Beuermann K. & Weichhold M., 1999, The Surface Brightness of Late-Type Main-Sequence Stars and the Distances to CVs, *ASP Conference Series*, **157**, 283

[11] Beuermann K., Thomas H.-C. & Schwope A.D., 1988 EXO 033319-2554.2 - A 55-MG eclipsing AM Herculis binary, *Astronomy & Astrophysics*, **195**, L15

[12] Beuermann K., Thomas H.-C., Giommi P. & Tagliaferri G., 1987, EXO 023432-5232.3 - A new 114-minute probable AM-Herculis-type binary, *Astronomy & Astrophysics*, **175**, L9

[13] Biermann, P., Schmidt, G. D., Liebert, J., Tapia, S., Strittmatter, P. A., West, S., Stockman, H. S., Kuehr, H. & Lamb, D. Q.,1985, The new eclipsing magnetic binary system E 1114 + 182, *Astrophysics Journal*, **293**, 303

[14] Bridge C. M., Cropper M., Ramsay G., Perryman M. A. C., de Bruijne J. H. J., Favata F., Peacock A., Rando N. & Reynolds, A. P., 2002, STJ observations of the eclipsing polar HU Aqr, *Mon. Not. R. Astron. Soc*, **336**, 1129

[15] Buckley D.A.H., 2001, Frist Light Instrumentation for the SALT, *ASP Conference Series*, **232**, 386

[16] Buckley D.A.H., Ferrario L., Wickramasinghe D.T. & Bailey J.A., 1998, Polarimetry of the Eclipsing Polar RX J0929.1-2404, *Mon. Not. R. Astron. Soc.*, **295**, 899

[17] Burwitz V., Reinsch K., Beuermann K. & Thomas H.-C., 1999, RX J0501.7-0359: A New ROSAT Discovered Eclipsing Polar in the Period Gap, *ASP Conference Series*, **157**, 127

[18] Chandrasekhar S., 1950, Radiative Transfer, Oxford University Press, Oxford

[19] Chanmugam G., 1987, Radio Emission from Cataclysmic Variables, *Astrophysics and Space Science*, **130**, 53

[20] Ciardi D.R., Howell S.B., Dhillon V.S., Wagner R.M., Hauschildt P.H. & Allard F., 1998, Observations of the Polar ST Leonis Minoris during an Extreme Low State: Identification of the Secondary Star, *PASP*, **110**, 1007

[21] Cropper M.S., 1985, Simultaneous Linear and Circular Polarisation of EF Eri, *Mon. Not. R. Astron. Soc.*, **212**, 709

[22] Cropper M.S., 1990, The Polars, *Space Science Reviews*, **54**, 195

[23] Cropper M.S., 1997 Polarization in the Hidden Pole AM Her System EXO 032957-2606.9, *Mon. Not. R. Astron. Soc.*, **289**, 21

[24] Cropper M., Menzies J.W. & Tapia S., 1986, E1405-451 - Three seasons of polarimetry and photometry, *Mon. Not. R. Astron. Soc.*, **218**, 201

[25] Cropper M. & Wickramasinghe D.T., 1993, Cyclotron humps in AM HER systems. V - Two poles in DP Leo, *Mon. Not. R. Astron. Soc.*, **260**, 696

[26] Davidson K. & Ostriker J.P., 1973, Neutron-Star Accretion in a Stellar Wind: Model for a Pulsed X-Ray Source, *Astrophys. J.*, **179**, 585

[27] Downes R.A., Webbink R.F., Shara M.M., Ritter H., Kolb U. & Duerbeck, H.W., 2001, A Catalog and Atlas of Cataclysmic Variables: The Living Edition, *Publ. Astron. Soc. Pac.*, **113**, 764

[28] Dubkova D.N., Kudryavtseva N.A. & Hirv A., 2003, The Light Curve of the New Cataclysmic Variable SDSS J015543.40-002807.2, *International Bulletin on Variable Stars*, **5389**, 1

[29] Eracleous M., Halpern J.P. & Patterson J., 1991, X-ray spectra of cataclysmic variables from the Einstein Observatory, *Astrophys. J.* **382**, 290

[30] Ferrario L. & Wickramasinge D.T., 1990, Arc-shaped cyclotron emission regions in AM Herculis systems, *The Astrophysical Journal*, **357**, 582

[31] Ferrario L., Wickramasinghe D.T., Bailey J. & Buckley D.A.H., 1995, H 1752+08: the lowest field AM Herculis system?, *Mon. Not. R. Astron. Soc.*, **273**, 17

[32] Ferrario L., Wickramasinghe D.T., Bailey J., Tuohy I.R. & Hough J.H., 1989, EXO 033319-2554.2: an Eclipsing AM Herculis System Showing Cyclotron Emission Features, *Astrophys. J*, **337**, 832

[33] Ferrario L., Wickramasinghe D.T. & Schmidt G., 2003, Analysis of new spectropolarimetric data of AR UMa, *Mon. Not. R. Astron. Soc.*, **338**, 340

[34] Greiner J., Remillard R.A. & Motch C., 1998, The X-ray Stream-Eclipsing Polar RX J1802.1+1804, *A& A*, **336**, 191

[35] Hakala P.J.,1995, Accretion stream mapping in eclipsing polars. an application of MEM and genetic optimisation, *A & A*, **296**, 164

[36] Harrop-Allin M.K., Cropper M., Hakala P.J., Hellier C. & Ramseyer T., 1999, Indirect Imaging of the Accretion Stream in Eclipsing Polars - II. HU Aquarii, *Mon. Not. R. Astron. Soc.*, **308**, 807

[37] Harrop-Allin M.K., Hakala P.J. & Cropper M., 1999. Indirect Imaging of the Accretion Stream in Eclipsing Polars - I. Method and Tests, *Mon. Not. R. Astron. Soc.*, **302**, 362

[38] Harrop-Allin M.K., Hakala P.J. & Cropper M., 2001, Indirect Imaging of the Accretion Stream in Eclipsing Polars - III. HU Aquarii low state, *Mon. Not. R. Astron. Soc.*, **326**, 788

[39] Hellier C., 2001, Cataclysmic Variable Stars: How and Why they Vary, Springer-Praxis Books in Astronomy and Space Science

[40] Horne K., 1985, Images of Accretion Discs. I - The Eclipse Mapping Method, *Mon. Not. R. Astron. Soc.*, **213**, 129

[41] Hsu H.-C. & Breger M., 1982, On Standard Polarized Stars, *The Astrophysical Journal*, **262**, 732

[42] King A.R. & Lasota, J.-P., 1984, The origin of the high and low luminosity states in magnetic cataclysmic variables, *Astronomy and Astrophysics*, **140**, L16

[43] Kolb U. & Baraffe I., 1999, The CV Period Minimum, *ASP Conference Series*, **157**, 273

[44] Kube J., Gänsicke B.T. & Beuermann K., 2000, Eclipse mapping of the accretion stream in UZ Fornacis, *A & A*, **356**, 490

[45] Lamb F.K., 1989, in *Timing Neutron Stars*, eds. H. Ögelman & E.P.J. van den Heuvel, Kluwer, p. 649

[46] Lamb D.Q. & Masters A.R., 1979, X and UV Radiation from Accreting Magnetic Degenerate Dwarfs, *Astrophys. J.*, **234**, L117

[47] Marsh T.R. & Horne K., 1998, Images of accretion discs. II - Doppler tomography, *Mon. Not. R. Astron. Soc*, **235**, 269

[48] Meggitt S.M.A & Wickramasinghe D.T., 1982, The Polarization Properties of Magnetic Accretion Columns, *Mon. Not. R. Astron. Soc*, **198**, 71

[49] Mukai K., 1988, Accretion streams in AM HER type systems, *Mon. Not. R. Astron. Soc.*, **232**, 175

[50] Nauenberg M., 1972, Analytic Approximations to the Mass-Radius Relation and Energy of Zero-Temperature Stars, *Astrophys. J.*, **175**, 417

[51] O'Donoghue D.,1995, High Speed CCD Photometry, *Baltic Astr.*, **4**, 517

[52] Osaki Y., 1974, An Accretion Model for the Outbursts of U Geminorum Stars, *Publ. astr. Soc. Japan*, **26**, 429

[53] Pavelin P.E., Spencer R.E. & Davis R.J., 1994, A 5-GHZ Radio Survey of Magnetic Cataclysmic Variables, *Mon. Not. R. Aston. Soc*, **269**, 779

[54] Piirola V., Reiz A. & Coyne G.V., 1987, Five-colour (UBVRI) polarimetry of H0139-68 = BL Hydri, *Astronomy & Astrophysics*, bf 185, 189

[55] Perryman M. A. C., Cropper M., Ramsay G., Favata, F., Peacock A., Rando N. & Reynolds, A., 2001, High-speed energy-resolved STJ photometry of the eclipsing binary UZ For, *Mon. Not. R. Astron. Soc.*, **324**, 899

[56] Perryman M. A. C., Foden C. L.& Peacock, A., 1993, Optical photon counting using superconducting tunnel junctions, *Nuclear Instruments and Methods in Physics Research Section A* , **325**, 319

[57] Potter. S.B., 1998, PhD Thesis, Univ. London

[58] Rando N., Verveer J., Andersson S., Verhoeve P., Peacock A., Reynolds A., Perryman M. A. C. & Favata F., 2000, S-Cam: A spectrophotometer for optical astronomy: Performance and latest results. *Review of Scientific Instruments*, **71**, 4582

[59] Ramsay G., 2000, Determining the Mass of the Accreting White Dwarf in Magnetic Cataclysmic Variables using RXTE data, *Mon. Not. R. Astron. Soc.*, **314**, 403

[60] Ramsay G. & Wheatley P.J., 1998. Spectroscopic Observations of the Eclipsing Polar MN Hya (RX J0929-24), *Mon. Not. R. Astron. Soc.*, **301**, 95

[61] Remillard R.A., Stroozas B.A., Tapia S. & Silber A., 1991, The eclipsing AM Herculis variable H1907 + 690, *Astrophys. J*, **379**, 715

[62] Rucinski S.M., 1984, Can activity of the secondary component explain the emission-line spectra of cataclysmic binaries?, *Observatory*, **104**, 259

[63] Salvi, N., Ramsay, G., Cropper M., Buckley D.A.H. & Stobie R.S., 2002, Indirect imaging of the accretion stream in eclipsing polars - IV. V895 Cen, *Mon. Not. R. Astron. Soc.*, **331**, 488

[64] Schmidt G.D. & Stockman H.S., 2001, Time-Resolved Hubble Space Telescope Spectroscopy of Four Eclipsing Magnetic Cataclysmic Variables, *The Astrophysical Journal*, **548**, 410

[65] Schmidt G.D., Ferrario L., Wickramasinghe D.T. & Smith P.S., 2001, The Cyclotron Fundamental Exposed in the High-Field Magnetic Variable V884 Herculis, *The Astrophysical Journal*, **553**, 823

[66] Schmidt G.D., Szkody P., Smith P.S., Silber A., Tovmassian G., Hoard D.W., Gänsicke B.T. & de Martino D., 1996, AR Ursae Majoris: The First High-Field Magnetic Cataclysmic Variable, *The Astrophysical Journal*, **473**, 483

[67] Schwope A.D., 2001, Tomography of Polars, in Boffin H.M.J., Steeghs D. & Cuypers J., eds, Lecture Notes in Physics Vol. 573, p.127

[68] Schwope A. & Mengel S., 1997, Phase-resolved spectroscopy and photometry of the eclipsing polar EP Draconis (=H1907+690), *Astronomische Nachrichten*, **318**, 25

[69] Schwope A.D., Beuermann K. & Thomas H.-C., 1990, Cyclotron radiation in UZ Fornacis (=EXO033319 - 2554.2) in a low state of accretion *Astronomy & Astrophysics*, **230**, 120

[70] Schwope A.D., Thomas H.-C. & Beuermann K., 1993, Discovery of the Bright Eclipsing Polar RX:J2107.9-0518, *Astronomy & Astrophysics*, **271**, L25

[71] Schwope A.D., Schwarz R., Sirk M. & Howell S.B., 2001, The Soft X-Ray Eclipses of HU Aqr, *Astronomy & Astrophysics*, **375**, 419

[72] Schwope A.D., Schwarz R., Staude A., Heelein C., Horne K. & Steeghs D., 1999, Tomography of Polars, *ASP Conference Series*, **157**, 71

[73] Serkowski K., 1962, Polarization of Starlight, *Advances in Astronomy and Astrophysics*, **1**, 290

[74] Serkowski K., 1974, Planets, Stars and Nebulae studied with Photopolarimetry, p. 135, ed. Gehrels T., University of Arizona Press. Tucson, Arizona

[75] Shafter A.W., Reinsch K., Beuermann K., Misselt K.A., Buckley D.A.H., Burwitz V. & Schwope A.D., 1995, RX J0515.6+0105: an unusual, eclipsing, magnetic cataclysmic variable, *Astrophys. J*, **499**, 917

[76] Sirk M.M. & Howell S.B., 1998, The Three-Dimensional Structure of Extreme-Ultraviolet Accretion Regions in AM Herculis Stars: Modeling of Extreme-Ultraviolet Photometric and Spectroscopic Observations, *The Astrophysical Journal*, **506**, 824

[77] Smith D.A. & Dhillon V.S.,1998, The Secondary Star in Cataclysmic Variables and Low-Mass X-Ray Binaries, *Mon. Not. R. Astron. Soc.*, **301**, 767

[78] Stobie R.S., Okeke P.N., Buckley D.A.H., O'Donoghue D., 1996, EUVE J1429-38.0: an eclipsing polar, *Mon. Not. R. Astron. Soc.*, **283**, L127

[79] Szkody P. et al., 2002, Cataclysmic Variables from the Sloan Digital Sky Survey. I. The First Results, *The Astronomical Journal*, **123**, 430

[80] Szkody P. et al., 2003, Two Rare Magnetic Cataclysmic Variables with Extreme Cyclotron Features Identified in the Sloan Digital Sky Survey, *The Astrophysical Journal*. **583**, 902

[81] Tovmassian G.H., Szkody P, Greiner J., Vrielmann S.,Kroll P., Howell S., Saxton R., Ciardi D., Mason P.A. & Hastings N.C., 1999, High Spectral Time Resolution Observations of the Eclipsing Polar RX J0719.2+6557, *ASP Conference Series*, **157**, 133

[82] Visvanathan N. & Wickramasinge D.T., 1981, Vv-Puppis in an Active Phase, *Mon. Not. R. Astron. Soc.*, **196**, 275

[83] Vrielmann S. & Schwope A.D.,2001, Accretion Stream Mapping of HU Aquarii, *Mon. Not. R. Astron. Soc.*, **322**, 269

[84] Vrielmann S. & Schwope A.D.,1999, Accretion Stream Mapping, *ASP Conference Series*, **157**, 93

[85] Warner B., 1995, Cataclysmic Variable Stars, Cambridge Astrophysics Series 28, Cambridge University Press

[86] Webbink R.F. & Wickramasinghe D.T., 2002, Cataclysmic Variable Evolution: AM Her Binaries and the Period Gap, *Mon. Not. R. astron. Soc.*, **335**, 1

[87] Wickramasingh D.T. & Ferrario L., 2002, The high field magnetic CVs, *ASP Conference Series*, **261**, 82

[88] Woudt P.A., Warner B. & Pretorius M.L., 2004, High-speed photometry of faint cataclysmic variables - IV. V356 Aql, Aqr1, FIRST J1023+0038, H? 0242-2802, GI Mon, AO Oct, V972 Oph, SDSS 0155+00, SDSS 0233+00, SDSS 1240-01, SDSS 1556-00, SDSS 2050-05, FH Ser, *Mon. Not. R. Astron. Soc*, **351**, 1015

[89] Wright A.E., Cropper M.S., Stewart R.T., Nelson G.J. & Slee O.B., 1988, Detection of the AM Her Type Cataclysmic Variable V843 Cen at Radio Wavelengths ,*Mon. Not. R. Aston. Soc*, **231**, 319